Thrust ramps within MTDs initiate within competent horizons in the hangingwall of the underlying detachment.

Within MTDs, the spacing of thrust ramps and thickness of the thrust sequence display a ~ 5:1 ratio.

Thrust systems within MTDs display greater variations in hangingwall and footwall cut-offs (or stretch) than in lithified rocks.

Thrust systems within MTDs broadly ‘balance’, although heterogeneous lateral compaction increases by ~10% towards the surface.

Critical taper angle in MTDs may be an order of magnitude less than in accretionary complexes and lithified rocks.

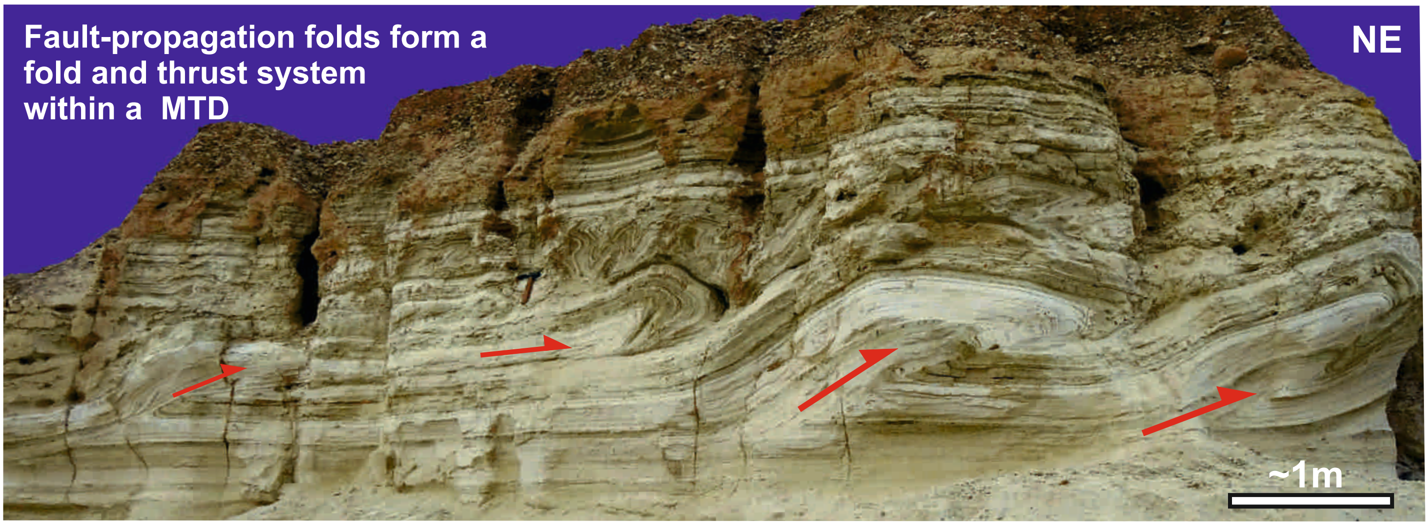

Fault-propagation folds form a fold and thrust system within a MTD
NE
~1m

Fold and thrust systems in Mass Transport Deposits.

G.I. Alsop[1], S. Marco[2], T. Levi[3], R. Weinberger[3, 4]
1) Department of Geology and Petroleum Geology, School of Geosciences,
University of Aberdeen, Aberdeen, UK. (e-mail: Ian.Alsop@abdn.ac.uk)
2) Department of Geosciences, Tel Aviv University, Israel.
3) Geological survey of Israel, Jerusalem, Israel.
4) Department of Geological and Environmental Sciences, Ben Gurion University of the Negev, Beer Sheva, Israel.

Abstract

Improvements in seismic reflection data from gravity-driven fold and thrust systems developed in offshore Mass Transport Deposits (MTDs) reveal a number of significant features relating to displacement along thrusts. However, the data are still limited by the resolution of the seismic method, and are unable to provide detail of local fold and thrust processes. Investigation of exceptional gravity-driven contractional structures forming part of MTDs in lacustrine deposits of the Dead Sea Basin, enables us to present the first detailed outcrop analysis of fold and thrust systems cutting unlithified 'soft' sediments. We employ a range of established geometric techniques to our case study, including dip isogons, fault-propagation fold charts and displacement-distance diagrams previously developed for investigation of thrusts and folds in lithified rocks. Fault-propagation folds in unlithified sediments display tighter interlimb angles compared to models developed for lithified sequences. Values of stretch, which compares the relative thickness of equivalent hangingwall and footwall sequences measured along the fault plane, may be as low as only 0.3, which is significantly less than the minimum 0.5 values reported from thrusts cutting lithified rocks, and reflects the extreme variation in stratigraphic thickness around thrust-related folds. We suggest that the simple shear component of deformation in unlithified sediments may modify the forelimb thickness and interlimb angles to a greater extent than in lithified rocks. The average spacing of thrust ramps and the thickness of the thrust sequence display an approximate 5:1 ratio across a range of scales in MTDs. In general, thicker hangingwall and footwall sequences occur with larger thrust displacements, although displacement patterns on thrusts cutting unlithified (yet cohesive) sediments are more variable than those in lithified rocks. Line-length restoration of thrust systems in MTDs reveals 42% shortening, which reduces to 35% in overlying beds. A 23% reduction in shortening by folding and thrusting along individual thrusts suggests that heterogeneous lateral compaction may increase by ~10% towards the sediment surface. Thrust systems cutting unlithified sediments display distinct steps in cumulative displacement-distance plots representing increased rates of slip along the floor thrust, while displacement-distance plots along individual thrusts also reveal 'horizontal steps' relating to lithological variation. Competent units cut by thrust ramps may display the greatest displacement, which then progressively reduces both upward and sometimes downward along the ramp. This relationship demonstrates that ramps do not necessarily propagate upwards from the underlying flat as in some traditional models, but rather initiate by offset of competent horizons in the hangingwall of the detachment. Critical taper angles in MTDs may be an order of magnitude less than in accretionary complexes or lithified rocks. Overall, thrusts cutting unlithified sediments in MTDs display more variable displacement, and more pronounced displacement gradients toward fault tips, compared to thrusts cutting lithified sequences.

Keywords: Mass Transport Deposits, thrusts, folds, slumping, Earthquakes, Dead Sea Basin

1. Introduction

The geometry and kinematics of large-scale fold and thrust belts generated by gravity-driven movement of sediments down continental slopes is becoming increasingly apparent from improved seismics across such structures (e.g. Corredor et al., 2005; Bull et al., 2009; Butler and Paton, 2010, de Vera et al. 2010; Morley et al., 2011; Jackson, 2011; Peel, 2014; Scarselli et al., 2016; Reis et al., 2016). However, whilst seismics may provide a clear overview of linked upslope (extensional) and downslope (contractional) domains within Mass Transport Deposits (MTDs) (e.g. Frey Martinez et al., 2005; Armandita et al., 2015), they are still limited in their ability to image complex and local detail (e.g. Jolly et al., 2016). Although exhumed examples of now lithified MTDs containing 'soft-sediment' fold and thrust systems provide some detail (see Maltman, 1984, 1994 for definitions), they suffer from potential changes in geometries due to compaction and lithification, possible later tectonism, and an increasing disconnect of ancient systems from their palaeo-geographic setting (e.g. see Korneva et al., 2016; Sobiesiak et al., 2016). In order to provide a detailed analysis of complex fold and thrust geometries associated with downslope movement of unlithified sediments within MTDs, we utilise relatively recent, late Pleistocene, decametric- to km-scale structures, which are fully exposed around the Dead Sea Basin, and for which the palaeo-geography is still evident today (Fig. 1).

In this study, we employ well-established techniques developed during many decades of structural analysis of fold and thrust systems in lithified rocks, and apply them to gravity-driven thrusts and associated fault-propagation folds cutting unlithified sediments. A fault-propagation fold is simply defined by Fossen (2016, p.366) as a fold that "forms above the tip-line of a thrust to accommodate the deformation in the wall rock around the tip" (see also Chapman and Williams, 1984; Ramsay and Huber, 1987, p.558; Suppe and Medwedeff, 1990). In order to undertake a robust and detailed investigation of fold and thrust systems, we use techniques such as fault-propagation fold charts (e.g. Jamison, 1987), dip-isogon analysis of fault-propagation folds (e.g. Ramsay, 1967), and restoration and 'balancing' of thrust systems (e.g. see Butler, 1987; Fossen 2016, p.441). A key element of our analysis are displacement-distance graphs that have been widely used for more than 30 years to analyse displacement gradients along both extensional and contractional faults cutting lithified rocks (Williams and Chapman, 1983; Chapman and Williams, 1984, 1985; Alonso and Teixell, 1992; Ferrill et al., 2016). However, similar techniques have rarely been applied to faults cutting unlithified sediments. A notable exception is the work of Muraoka and Kamata (1983), who analysed displacement gradients along minor normal faults cutting Quaternary lacustrine sediments in Kyushu, Japan. Similar detailed displacement-distance analysis has not been performed on contractional faults in unlithified sediments, and we therefore focus our attention on analysis of such soft-sediment thrusts.

Our overall aim is to describe and quantify thrust and fault-propagation fold geometries that form during soft sediment deformation associated with gravity-driven downslope slumping of sediments in MTDs. Such patterns may help illustrate the role that different lithologies play during slumping, and potentially highlight general differences between displacement on faults cutting lithified rocks and unlithified sediments. We raise a number of research questions related to thrusting of unlithified sediments including:

i) How does the thickness of stratigraphic cut-offs compare across thrusts in MTDs?

ii) How do fault-propagation folds in sediments compare to those in lithified rocks?
iii) Where do thrust ramps initiate during slumping in MTDs?
iv) What controls the spacing of thrust ramps in MTDs?
v) Do thrust systems in MTDs 'balance' and what values of lateral compaction are attained in sediments?
vi) Do linked thrust systems in MTDs undergo constant rates of slip?
vii) What influences patterns of displacement along individual thrusts in MTDs?
viii) How do critical taper angles in MTDs compare to those in accretionary complexes?

2. Geological setting

The Dead Sea Basin is a pull-apart basin developed between two left-stepping, parallel fault strands that define the sinistral Dead Sea Fault (Garfunkel, 1981; Garfunkel and Ben-Avraham, 1996) (Fig. 1a, b). The Dead Sea Fault has been active since the Early to Middle Miocene (e.g. Bartov et al., 1980; Garfunkel, 1981) including during deposition of the Lisan Formation in the late Pleistocene (70-15 ka) (Haase-Schramm et al. 2004). During this time numerous earthquakes triggered co-seismic deformation (e.g. Weinberger et al., 2016) as well as soft-sediment deformation and slumping in the Lisan Formation (e.g. El-Isa and Mustafa, 1986; Marco et al., 1996; Alsop and Marco 2011; 2012a, 2012b, 2013, 2014, Alsop et al., 2016b). Analysis of drill cores from the depocentre of the Dead Sea reveals that the Lisan Formation is three times thicker than its onshore equivalent, largely due to the input of transported sediment and disturbed layers (Marco and Kagan, 2014). The fold and thrust systems observed onshore may ultimately form part of these larger MTDs that feed into the deep basin.

The Lisan Formation comprises a sequence of alternating aragonite-rich and detrital-rich laminae on a sub-mm scale. They are thought to represent annual varve-like cycles with aragonite-rich laminae precipitating from hypersaline waters in the hot dry summer, while winter flood events wash clastic material into the lake to form the detrital-rich laminae (Begin et al., 1974). Varve counting combined with isotopic dating suggests that the average sedimentation rate of the Lisan Formation is ~1 mm per year (Prasad et al., 2009). Seismic events along the Dead Sea Fault are considered to trigger surficial slumps and MTDs within the Lisan Formation, resulting in well-developed soft-sediment fold and thrust systems (Alsop and Marco, 2011; Alsop et al., 2016b). Breccia layers generated next to syn-depositional faults are also thought to be the product of seismicity (e.g. Marco and Agnon, 1995; Agnon et al. 2006). Detrital (mud-rich) horizons that are <10 cm thick and contain fragments of aragonite laminae are interpreted to be deposited from suspension following seismicity (e.g. Alsop and Marco 2012b). Individual slump sheets are typically <1.5 m thick and are capped by undeformed horizontal beds of the Lisan Formation, indicating that fold and thrust systems formed at the sediment surface (e.g. Alsop and Marco, 2011).

The slumps, together with the intervening undeformed beds within the Lisan Formation, are themselves cut by vertical clastic dykes (Marco et al., 2002) containing fluidised sediment sourced from underlying units during seismic events (e.g. Levi et al., 2006, 2008; Jacoby et al., 2015; Weinberger et al., 2016). Within the sedimentary injections, optically stimulated luminescence (OSL) for quartz give ages of between 15 and 7 ka (Porat et al., 2007), indicating brittle failure and intrusion after deposition of the Lisan Formation.

The slump systems around the Dead Sea Basin are developed on very gentle slopes of <1° dip and define an overall regional pattern of radial slumping associated with MTDs that are directed towards the depo-centre of the present Dead Sea Basin (Fig. 1c) (Alsop and Marco 2012b, 2013).

The Peratzim case study area (N 31º0449.6 E 35º2104.2) is located on the Am'iaz Plain, which is a downfaulted block positioned between the Dead Sea western border fault zone, which bounds the Cretaceous basin margin ~2 km to the west, and the upstanding10 km long ridge formed by the Sedom salt wall 3 km further east (e.g. Alsop et al., 2015, 2016a) (Fig. 1c, d). This area is ideal for investigating thrusts cutting unlithified sediments of MTDs as: 1) It is well exposed and accessible (using ladders) along incised wadi walls. 2) The varved lacustrine sequence permits high resolution mm-scale correlation of 'barcode-style' sequences across thrust faults. 3) The two main aragonite-rich and detrital-rich lithologies help simplify the mechanics in to a binary system of generally incompetent (aragonite-rich) and relatively competent (detrital-rich) units. This dichotomy allows us to more easily analyse the control of lithological variation on thrusting (e.g. Alsop et al., 2016b). 4) Relatively recent (70-15 ka) slumping associated with MTDs permits a greater degree of certainty regarding thrust transport and palaeoslope directions (Alsop and Marco, 2012b). 5) The nature of the surficial slumping, where overburden has not exceeded a few metres (e.g. Alsop et al., 2016b), removes many doubts including complications associated with changes in geometries and angles arising from subsequent compaction of sediments. The Lisan Formation is considered to have been water-saturated at the time of deformation, while the lack of subsequent compaction means that the present water content is still ~ 25% (Arkin and Michaeli, 1986).

3. Orientation and geometry of fold and thrust systems

It has long been recognised that slump folds and thrusts display distinct and systematic relationships with respect to the palaeoslope upon which they developed (e.g. Woodcock, 1976a, b; 1979; Strachan and Alsop, 2006; Debacker et al., 2009; van der Merwe et al., 2011; Garcia-Tortosa et al., 2011; Sharman et al., 2015; Ortner and Kilian, 2016). Alsop and Marco (2012b) employed a range of different geometric techniques to establish overall slump transport directions within MTDs around the Dead Sea Basin. The orientation of the transport direction, and associated palaeoslope, was inferred to be toward 045° in the Peratzim area. Folds and thrusts throughout the study area are dominated by layer-parallel shearing, resulting in the trends of fold hinges and strikes of thrust planes forming normal to transport (see Alsop and Holdsworth 1993; 2007; Alsop and Marco, 2011; 2012b for details). Subsequent work (Alsop et al., 2016b) has demonstrated that six individual MTDs are exposed at Peratzim, and although fold data from individual slump sheets may locally vary, the overall transport direction is still considered to be northeast toward the basin depocentre. Our work focuses on slumps 4, 5 and 6 in the Alsop et al. (2016b) sequence. The structures we show are typical of the slumps in this locality, where perhaps unparalleled examples of thrusts and associated fault-propagation folds are developed in unlithified sediments.

In the present study, a series of outcrops through fold and thrust sequences were specifically chosen such that the cross section views along incised wadi cuts are subparallel to the locally calculated transport directions (Fig. 2a, b, c). This approach involved the use of a ladder to reach and measure otherwise inaccessible structures high up wadi walls, facilitating detailed geometric analysis of thrusts and folds cutting unlithified sediments. These wadi cuts contain excellent examples of thrusts on a metre scale, together with fault-propagation folds developed in the immediate hangingwalls toward the thrust tips (Fig. 2a, b, c).

In slump 5 (Fig. 2a), the associated stereonet data (Fig. 2d) shows that the wadi cutting trends 045° while the normal to the mean fold hinge is 047°, and the normal to the mean thrust-strike is 040°. The section is thus within 5° of the calculated transport direction using a range of techniques (Alsop and Marco, 2012b). In slump 4 (Fig 2b, e), the wadi cutting trends 090° while the normal to the mean fold hinge is 100°, and the normal to the mean thrust-strike is 095°. The section is thus within 10° of calculated MTD transport. In another exposure from slump 4 (Fig 2c, f), the wadi cutting trends 090° while the normal to the mean fold hinge is 094°, and the normal to the mean thrust-strike is 072°. All sections are thus within 10° of calculated transport, and we do not consider these slight obliquities between trends of wadi cuttings and mean transport to be sufficient to skew our structural analysis. The detailed measurements of fold and thrust parameters are therefore true representatives of the actual geometries, and are not overly influenced by potential oblique 'cut effects'.

In general, Alsop and Marco (2011) recognised that the linked thrusts and fault-propagation folds at Peratzim broadly follow a 'piggyback' sequence, whereby new thrusts develop in the footwall of existing thrusts, resulting in a back-steepening and rotation of the older thrust and an overall forward or downslope propagating system of thrusts (e.g. Fig. 2b, g, h). Some evidence also exists for out-of-sequence thrusting, where thrusts initiated upslope cut through earlier piggyback thrusts preserved in their footwall (Fig. 2g, h).

4. Relationship of stratigraphic thickness to thrust displacement and spacing

4.1. Thickness of stratigraphic sequences in the footwall and hangingwall of a thrust

The stratigraphic thickness of a sequence is measured orthogonal to bedding in an area removed from thrusts and folds (Fig. 3). Analysis of thrusts in the study area reveals that an overall general correlation exists between the thickness of the thrusted stratigraphic sequence, and the maximum displacement along the thrust (Fig. 4a). The hangingwall and footwall thickness of a stratigraphic package is measured parallel to transport along the thrust ramp, and is defined by the stratigraphic cut-offs above and below the thrust plane, respectively (Fig. 3). In the study area, the hangingwall thickness of a stratigraphic interval is consistently less than the equivalent sequence in the footwall of a thrust, due to folding and shearing of the hangingwall stratigraphy into anticlines (Fig 4b). This relationship applies across a range of scales from cm to metres. The mean hangingwall and footwall thicknesses from different imbricate sequences at different localities may also be calculated, and compared with the mean displacement across the thrusts (Fig. 4c). Hangingwall thicknesses are consistently less than equivalent footwall sequences, with greater thicknesses generally marked by increasing displacement (Fig. 4c).

4.2. Relative stretch

The relative stretch (ε_r) can be calculated by measuring the ratio of the measured lengths of the hangingwall (l_h) and footwall (l_f) cut-offs parallel to the thrust, (where $\varepsilon_r = l_h$ over l_f) (e.g. Noble and Dixon, 2011, p.72) (Fig. 3). Models run by Noble and Dixon (2011) showed that folding of sediments in the hangingwall increases relative dips and thereby reduces the length of the hangingwall along the thrust ramp, such that smaller relative stretch indicates a greater amount of fold shortening accrued during structural development.

In Peratzim, hangingwall lengths (l_h) are consistently shorter than those in the footwall (l_f), with relative stretch values as low as 0.4 attained in the analysed fault-propagation folds (Fig. 4d). Elsewhere in the study area, even smaller values of 0.3 are locally achieved. Values of stretch within fault-propagation folds generally reduce as hangingwall thickness reduces (Fig. 4d) and displacement increases (Fig. 4e). In some cases, pronounced displacement gradients towards thrust tips result in 400 mm of displacement reducing to zero along a distance of 200 mm of fault, with overlying beds folded, but not thrust. Rapidly diminishing displacement indicates greater slip/propagation ratios and large relative stretch i.e. fault-propagation folding (Noble and Dixon, 2011, p.73).

4.3. Spacing of thrust ramps

Liu and Dixon (1995) measured the spacing between thrust ramps in lithified rocks, with spacing defined as the bed length between adjacent thrust ramps, when measured parallel to transport (Fig. 3). Using this approach, we find a broad correlation between spacing of thrust ramps and the thickness of the unlithified stratigraphic sequence cut by the thrusts (Fig. 4f). In general, the ramp spacing increases by approximately 1 m for each additional 200 mm of sequence thickness, suggesting a general 5:1 spacing/thickness ratio (Fig. 4f). This correlation is in general agreement with thrust systems cutting lithified rocks across a variety of scales (Liu and Dixon, 1995).

5. Analysis of thrusts and folds

5.1. Dip-isogon analysis of thrust-related folds

The dip-isogon method is a well-established technique of fold classification in lithified rocks (e.g. Ramsay, 1967, p.363). We use this method to analyse fault-propagation folds developed in the hangingwall of thrusts, and compare fold geometries formed in aragonite-rich and detrital-rich units (Fig. 5a). Our analysis includes data from both the upper and lower limbs of the hangingwall anticline, and shows that folds within aragonite-rich units display gently convergent to parallel isogons that typically define Class 1C to Class 2 similar folds (Ramsay, 1967; Fossen, 2016, p.263) (Fig. 5a, b). However, folds within a 10 cm thick detrital-rich marker display strongly convergent isogons that resemble Class 1B or parallel folds, although they also stray into the upper part of Class 1C (Fig. 5a, b). These results show that fold styles are consistent with the detrital-rich marker forming a more competent horizon, compared to the surrounding aragonite-rich units. The greater relative competence of the 10 cm thick detrital unit at the time of deformation is thus demonstrated by a more parallel (Class 1B) style of folding.

We have further investigated variations in bedding thickness around fault-propagation folds in Slump 5 (Fig. 2a) by measuring the % of thickening or thinning of fold forelimbs when compared to the thickness of the adjacent backlimb (see Fig. 3, Jamison, 1987 and

Fossen, 2016, p.363 for definitions) (Fig. 5c). Analysis reveals that relative thinning of the forelimb is developed in folds with interlimb angles of <60°, whereas folds displaying pronounced (>60%) thickening of the forelimb have interlimb angles of >90° (Fig. 5c). These relationships suggest that for thrusts cutting unlithified sediments, interlimb angles of fault-propagation folds are controlled by forelimb thickening or thinning.

5.2. Fault-propagation fold charts

As noted previously, fault-propagation folding is a commonly used term to describe folds formed above upwardly propagating thrust faults (e.g. Suppe and Medwedeff, 1990; Ferrill et al., 2016). Where a fault tip ceased to propagate, then "continued fault displacement is accommodated by folding within incompetent or mechanically layered strata beyond the fault tip" (Ferrill et al., 2016, p.10). Jamison (1987) recognised that the interlimb angle of such fault-propagation folds was a function of ramp angle as measured from the flat of the thrust, (see Fig. 3) and the amount of forelimb thickening or thinning. For his analysis, Jamison (1987) assumed that bedding maintained a constant thickness, apart from in the forelimb where either thickening or thinning could occur.

Fault-propagation folds at Peratzim broadly follow the patterns for predicted thickening and thinning of limbs in the fold model of Jamison (1987) (Fig. 6a, b, c). However, in each case, the observed amount of forelimb thinning is significantly less than predicted, while the amount of forelimb thickening is more variable, although tending to be greater than predicted (Fig. 6a, b, c). These relationships suggest that compared to the model, interlimb angles at Peratzim are too small, and/or ramp angles are too great. Due to the steep nature of the curves, variations in interlimb angles are most sensitive to changes. Folds which have undergone forelimb thickening have their interlimb angles significantly overestimated.

5.3. Balancing of thrust sections and lateral compaction

Restoration of displacement across thrust systems such that they 'balance' is an established and widely employed technique in both orogenic belts (e.g. see Butler, 1987; Fossen, 2016, p.441 and references therein) and also increasingly via seismic interpretation of gravity-driven offshore fold and thrust belts forming MTDs (e.g. Butler and Paton, 2010). In this study, a simple line-length balancing exercise across a well-developed fold and thrust system was undertaken (Fig. 7). Area balancing is not possible because the thickness of the original stratigraphic template is unknown due to continuous variations in detrital input from wadi flood events i.e. non layer-cake stratigraphy (Alsop et al., 2016b). As noted previously, folding of aragonite-rich layers results in similar (Class 2) folds that are interpreted as passive folds generated by simple shear (Fossen, 2016, p.268), while the adjacent detrital-rich marker defines a more parallel (Class 1B) folding consistent with flexural shear (Fig. 5a, b). Both fold styles largely preserve bed length (Fossen, 2016, p.445), and are therefore suitable for line-length balancing. Although some movement of sediment out of the plane of thrust transport cannot be entirely ruled-out (see Alsop and Marco, 2011), the analysed section was chosen because it lies within 5° of the calculated thrust transport direction (Fig. 2a, d). In addition, the general sequence of piggyback thrusting is well understood (e.g. Alsop and Marco, 2011), while the influence of subsequent compaction on thrust geometries can be largely ignored, as overburden above the thrust sequence did not exceed 3 m (Alsop et al., 2016b). Thus, while recognising the likely limitations, we mitigated against as many of these potential issues as possible when completing section restoration.

Our line-length balancing (Fig. 7a, b, c) shows that the percentage of thrust shortening increases down through the sequence, reaching ~40.6% in the lower blue marker, while the percentage of fold shortening increases upward through the sequence, reaching 9.3% in the top green marker (Table 1). The mismatch in restored line lengths indicates that there is 9.7% (3.8 m) of missing shortening from the restored lower blue up to the top green marker horizons (Fig. 7a, b, c, Table 1). This reduction is significant as it equates to a greater proportion of shortening which is missing (~23%), as compared to that which is actually observed in the form of folds in the top green marker (Fig. 7, Table 1). Given that the structures deform both the lower blue and top green markers without a sedimentary cap in between, this reduction in shortening up through the sequence is not the result of post-thrusting deposition. In summary, while fold and thrust sequences broadly 'balance', notable differences in amounts of thrust and fold shortening occur through the continuous stratigraphic package.

5.4. Cumulative displacement-distance graphs

Cumulative displacement-distance (CD-D) graphs were established by Chapman and Williams (1984) to measure thrust displacement, where shortening is accommodated in a linked-fault system that forms above a single floor thrust. A reference point is fixed where the leading imbricate thrust branches from the floor thrust (Chapman and Williams, 1984, p.124, their Fig. 4). In the case study, this imbricate thrust formed furthest downslope and is therefore the most northeasterly thrust ramp (T1) of each set of imbricates. The distance from this fixed reference point is then measured along the underlying floor thrust, to where each successive imbricate thrust branches from the floor thrust (T1 to T8 in Fig. 2). These distances are combined to form the cumulative distance on the horizontal axis of CD-D graphs. Displacement of a marker bed across each individual thrust imbricate is measured starting with the first thrust ramp (T1), and is then progressively combined with subsequent ramps (T1+T2 etc.) to create the cumulative displacement on the vertical axis of CD-D graphs.

We analysed 4 thrust systems cutting the unlithified sequence in the case study (Fig. 8). In the simplest situation involving relatively small displacements across thrusts cutting aragonite-rich units with minor detrital laminae, the cumulative displacement-distance (CC-D) graphs display linear profiles with a constant gradient (Fig. 8a, b). This indicates that displacement and distance are proportional, and represent a constant rate of slip along the floor thrust (Chapman and Williams, 1984).

However, where displacement increases, and / or stratigraphy becomes more varied with distinct detrital-rich units, then CD-D graphs along these thrust systems typically display more variable profiles marked by a distinct step (Fig. 8c, d). In both cases, analysis towards the downslope part of the system shows that cumulative displacement forms a steeper gradient when compared to greater distance along the thrust system (Fig. 8c, d). A slight step in the profile, where displacement increases proportionally more than distance along the thrust system, is developed in the restored central part (about 10 m from the start of the section in the NE) of exposed thrusts systems, before returning to more gentle gradients (Fig.

8c, d). In summary, the overall gradients of the two thrusts systems in the first 10 m of restored section are similar to one another, before the occurrence of a pronounced step representing an increase in relative displacement.

5.5. Displacement-distance graphs

Displacement-distance (D-D) graphs are widely employed in the analysis of faults cutting lithified rocks (e.g. Williams and Chapman, 1983; Ferrill et al., 2016). In this analysis, we measure the distance along the hangingwall of a thrust from a fixed reference point ('R' near the fault tip) to a marker horizon, and compare this distance with the displacement of that marker by measuring the amount of offset to the same horizon in the footwall (Muraoka and Kamata, 1983; Williams and Chapman, 1983) (Fig. 3). The process is then repeated for different markers along the fault length to create a displacement-distance (D-D) graph for that fault. In general, gentle gradients on D-D plots represent more rapid propagation of the thrust tip relative to slip, whereas steeper gradients represent slower propagation relative to slip (e.g. Williams and Chapman, 1983; Ferrill et al., 2016). In addition, displacement on faults is typically assumed to be time-dependent, resulting in older portions of faults accumulating the greatest displacement (e.g. Ellis and Dunlap, 1988; Hedlund, 1997; Kim and Sanderson, 2005). The point of maximum displacement on a D-D plot is therefore typically interpreted to represent the site of fault nucleation (e.g. Ellis and Dunlap, 1988; Peacock and Sanderson, 1996; Hedlund, 1997; Ferrill et al., 2016).

In the study area, we have measured displacement and distance along an incipient thrust that is cutting the ~ 10 cm thick detrital-rich 'orange' marker horizon in slump 5 (Fig. 9a, b). The displacement across the thrust is greatest (~ 60 mm) where it cuts the detrital horizon, and then reduces both up and down the thrust plane where it enters the relatively incompetent aragonite-rich units (Fig. 9a, b). A similar pattern is also observed where more fully-developed thrusts cut this same marker horizon (Fig. 9c, d), while thinner detrital horizons (highlighted in blue) also produce displacement maxima (Fig. 9e, f), or horizontal-steps in D-D graphs (Fig. 9c, d). As noted above, displacement maxima are considered to mark sites where faults initiate, and such sites are widely recognised where thrusts cut competent horizons in lithified rocks (e.g. Ellis and Dunlap, 1988; Ferrill et al., 2016). These D-D profiles support the competency contrasts between detrital-rich (relatively competent) and aragonite-rich (incompetent) units established by analysis of fold geometries of the same horizon (Fig. 5a, b).

As noted above, the greatest displacement may occur where thrusts cut the thicker (>10 cm) detrital-rich unit (Fig. 5, 9). However, in other cases, a simple deflection or horizontal step in the displacement-distance curve occurs where thrusts cut this detrital-rich unit (Fig. 9g-j). These steps in D-D graphs tend to develop where overall displacement along the thrust is larger (>2000 mm). This deflection in the D-D profile marks the point where more displacement occurs along the thrust than would be anticipated if displacement had continued to decrease systematically towards the fault tip (Fig 9g-j). The horizontal step marking more gentle gradients in the D-D plot suggests that the thick detrital-rich layer marks a distinct mechanical boundary.

In general, aragonite-rich units with thin detrital seams (< 1cm) display more linear profiles on D-D graphs, especially where displacement is relatively limited (<700 mm) (e.g.

Fig. 10a, b, c), although curves may get noticeably steeper toward the sediment surface and the fault tip (Fig. 10a, d, e). In some cases, D-D profiles may become highly irregular with several displacement peaks where thrusts with relatively modest displacement (< 800 mm) cut a series of detrital-rich units (Fig. 10a, f, g). In summary, where numerous thin detrital-rich horizons exist then displacement profiles tend to be more uniform and linear, although increases in displacement gradient are still observed towards the fault tip (Fig. 10a-g).

An opportunity to further investigate the influence exerted by detrital-rich units on variations in displacement profiles is provided by lateral sedimentary facies changes associated with input from wadi flood events (Alsop et al., 2016b). Thus, just 30 m further upslope towards the SW from Figure 10, the same slump system (slump 5 of Alsop et al., 2016b) cuts a sequence with thicker detrital-rich horizons, resulting in a very different set of D-D profiles (Fig. 11). The presence of thicker (~10 cm) detrital-rich units results in more pronounced steps and 'jumps' in displacement on D-D graphs (Fig. 11). The heterogeneity of the stratigraphic template thus influences displacement patterns along thrusts. However, differences in D-D profiles from adjacent thrusts that cut the same stratigraphy may also be pronounced (e.g. compare Figs 10c, e and g, or Figs 11c, e and g). As both thrust systems (Figs 10, 11) are associated with piggyback thrust sequences in the same slump horizon, then differences on D-D graphs may represent changes in displacement of these actual detrital-rich horizons. Alternatively, differences in D-D graphs may reflect other more nebulous variables linked to individual strain rates and fluid pressure / content. However, when analysing thrust interaction with stratigraphy (Fig. 11), it is apparent that the more irregular D-D profiles develop where the thrust has a larger displacement measured directly across thicker detrital-rich horizons (Fig. 11d, e). Variation in thrust displacement on D-D profiles may therefore not only reflect the point of initiation of the thrust, but also its continued development and that of associated fault-propagation folding during ongoing movement.

6. Discussion

6.1. How does the thickness of stratigraphic cut-offs compare across thrusts in MTDs?

As noted previously, relative stretch can be calculated by measuring the ratio of the measured lengths of the hangingwall and footwall cut-offs parallel to the thrust (Noble and Dixon, 2011, p.72), and reflects folding adjacent to the thrust (Fig. 3). Williams and Chapman (1983) recorded relative stretch values of between 0.5 and 0.89 from thrusts cutting lithified rocks, while general values of between 0.5 and 1 are quoted by Chapman and Williams (1984). Models of fold and thrust systems generated by Noble and Dixon (2011) record stretches of ~0.8, which are broadly equivalent to natural examples in lithified rocks. Williams and Chapman (1983, p.569) note that folds in the hangingwall form "at the leading edge of a propagating thrust due to a relatively fast slip rate on a relatively slowly propagating thrust". Within the study area, relative stretch values as low as 0.3 to 0.4 are recorded, with only a few thrusts that generated stretches greater than 0.7 (Fig. 4d, e). These values suggest a greater folding component within unlithified sediments compared to rocks, and is consistent with relatively fast slip on a relatively slowly propagating thrust in weak sediments. The observation that curves on D-D graphs are steeper toward the sediment surface (e.g. Figs. 9, 10, 11) is also consistent with lower stretch values marked by more pronounced hangingwall folding in the upper parts of thrusts.

Our study also shows that stratigraphic thickness generally correlates with displacement across thrust ramps (Fig. 4a, c). We suggest that thrusts with thinner overburden will simply ramp to the sediment surface before significant displacement has accumulated on individual thrusts. Thrusts that affect and cut a thicker stratigraphic sequence obviously remain more deeply buried, with consequent opportunity for greater displacement before surface breaching occurs. We therefore propose that it is proximity to the sediment surface that hinders large displacements accumulating on surficial thrusts.

6.2. How do fault-propagation folds in sediments compare to those in lithified rocks?

Interlimb angles of soft-sediment folds are less than anticipated in the model developed by Jamison (1987), and are significantly overestimated when using these charts that were developed for lithified rocks (Fig. 6a, b, c). Where incompetent aragonite-rich layers have been rotated and 'smeared' along the thrust plane, we infer that there has been additional components of thrust-parallel heterogeneous simple shear and pure shear (Alonso and Teixell, 1992). As noted by these authors, this thrust-parallel simple shear was not uniformly distributed along the thrust, but was concentrated in regions where thrusting was inhibited, such as thrust ramps or tip zones. It should also be noted that internal strain in the hangingwall of thrusts may be accommodated by layer-parallel shortening as well as folding, (e.g. Cooper et al., 1982; Chapman and Williams, 1985). Given the lack of evidence for thickening of sedimentary growth strata in the forelimb of folds, deformation is inferred to have occurred rapidly directly beneath the sediment surface.

Analysis of percentage thickening or thinning of forelimbs for fault-propagation folds at Peratzim reveals a strong correlation with interlimb angles (Fig. 5c). These relationships suggest that for thrusts cutting unlithified sediments, interlimb angles are a better indicator for forelimb thickening or thinning than ramp angles. We suggest that the simple shear component of deformation in unlithified sediments modifies the forelimb thickness and interlimb angles to a greater extent than in lithified rocks. The exact mechanical nature of aragonite- or detrital-rich horizons may also locally influence the resulting patterns of modification to limb thickness (e.g. Fig. 5a).

6.3. Where do thrust ramps initiate during slumping in MTDs?

Classical models of thrust displacement along ramp and flat systems assumed or implied that ramps propagate upwards from underlying floor thrusts that form flats (e.g. Rich, 1934; Boyer and Elliot, 1982; McClay, 2011; Fossen 2016, p.360). However, it has also been suggested that thrust ramps may nucleate above the main detachment, and propagate both upward and downward toward the underlying thrust flat (Eisenstadt and DePaor 1987, Ellis and Dunlap, 1988; Apotria and Wilkerson, 2002; Uzkeda et al., 2010; Ferrill et al., 2016; Dotare et al., 2016). This scenario is supported by analogue modelling, where Noble and Dixon (2011) noted that thrusts initiate in the lowermost competent unit of their models. Numerical modelling by Liu and Dixon (1995) also showed that stress concentrations are greatest at the base of the lowermost competent stratigraphic unit. They noted that "faults which ramp through these units are likely to merge with floor and roof thrusts" (Liu and Dixon, 1995 p.885).

It is generally considered that the greatest displacement will be preserved where the fault initiated (e.g. Ellis and Dunlap, 1988; Ferrill et al. 2016). At Peratzim, more offset is frequently developed across competent layers, consistent with the interpretation that ramps nucleate at these sites (Fig. 9c, d). In addition, where the sequence is relatively weakly deformed, only the competent layer is contractionally faulted, with displacement reducing up and down away from this horizon (Fig. 9a, b). Likewise, footwall synclines are typically best developed below the 'orange' marker horizon where ramps are interpreted to have initiated (e.g. Fig. 9a, e, g). Ferrill et al. (2016) suggested that footwall synclines develop due to the downward propagation of thrusts that initiate in overlying competent layers. The development of footwall synclines in our examples also suggests that thrust ramps initiated in competent horizons, and then mostly propagated up and down.

While points of maximum displacement on D-D graphs are considered to represent sites of fault initiation (Ellis and Dunlap, 1988; Ferrill et al., 2016), internal displacement minima along fault planes represent barriers to single fault propagation, or sites of fault linkage between originally separate minor faults. Such displacement minima may coincide with slight bends in the fault, separating two planar segments. Ellis and Dunlap (1988, p.189) noted that the apparent absence of multiple nucleation points on larger thrusts may indicate that any original displacement irregularities, reflecting initiation of original smaller faults, were overwhelmed and masked by subsequent large displacement on thrusts. More variable displacement profiles are indeed observed from thrusts with smaller overall offset in Peratzim (e.g. Fig. 9a, 9b, 10g). Overall, the D-D plots at Peratzim suggest that thrust ramps may have initiated in the competent horizon, and propagated up and down to intersect the floor thrust marking the basal detachment to the slump (see Eisenstadt and De Paor, 1987) (Fig. 12).

6.4. What controls the spacing of thrust ramps in MTDs?

Liu and Dixon (1995, p.875) noted that "thrust ramps exhibit a regular spacing linearly related to the thickness of strata involved in the duplex". They suggested that this spacing links to buckling instability, where the wavelength of dominant buckling controlled the ramp spacing. In the present study, our data are restricted to ramp spacing of <6 m and sediment thicknesses of <1 m, providing a general 5:1 ratio (Fig. 12). This value is similar to analysis of thrust sections presented by Gibert et al. (2005), where we calculated a sedimentary thickness to ramp spacing of 5.33 (where hangingwall thickness is ~ 1 m).

Analysis of seismic sections across gravity-driven fold and thrust belts though unlithified sediments in offshore Brazil (Zalan, 2005) provide a ratio of 4.73 where sediment thicknesses are ~700 m. Similar structures in the 'outer thrust system' of offshore Namibia (Butler and Paton, 2010) provide ratios of 4.7 when overburden reaches ~ 1 km. Slight variations in ratios may relate to thickening / thinning of layers that affects both thickness and length measurements of the layers. It appears therefore that the correlation between ramp spacing and thickness of strata originally recognised by Liu and Dixon (1995) in thrust systems cutting lithified rocks, can be applied to thrusts cutting unlithified sediments across a variety of scales in outcrop and seismic studies of MTDs.

6.5. Do thrust systems in MTDs 'balance' and what values of lateral compaction are attained in sediments?

Fold and thrust belts are typically considered to deform by thrusting, folding and layer-parallel shortening that equates to layer-parallel compaction in sediments (see Koyi et al. 2004 for a summary). Restoration of deformed sequences accounts for the thrusting and folding components, but calculations of layer-parallel compaction are typically hampered as this deformation develops pervasively on a grain scale. Layer-parallel compaction is therefore frequently a 'missing parameter' which is leftover after other more obvious structures have been measured and taken into account (for notable exceptions, see Coward and Kim, 1981; Fischer and Coward, 1982; Cooper et al., 1982). Estimates of layer-parallel shortening in orogenic fold and thrust belts are significant and vary from 15% (e.g. Morley, 1986; McNaught and Mitra, 1996) through to 20% in the Spanish Pyrenees (Koyi et al., 2004) and 33% in the Scottish Caledonides (e.g. Fischer and Coward, 1982).

Layer-parallel compaction is also interpreted from the analysis of seismic sections across large-scale offshore gravity-driven fold and thrust belts within MTDs, which reveals a mismatch in restoration of upper marker layers (that display less thrusting and folding than those lower down) (Butler and Paton, 2010). Butler and Paton (2010, p.9) attributed this mismatch to heterogeneous lateral compaction increasing (we calculate by up to 8%) in their upper layer. The restored fold and thrust systems in the case study display up to 41.8% shortening (Table 1). However, there is approximately 10% 'missing' contraction in the top green horizon that marks the upper portions of the thrusts (Fig. 7; Table 1). Although it is uncertain as to how much layer-parallel compaction affected the entire sequence, we suggest that this mismatch in contraction through the fold and thrust system may be accounted for by a ~10% increase in heterogeneous lateral compaction up through the sediment. This figure is not dissimilar to our estimate of an 8% increase in heterogeneous lateral compaction up through large-scale fold and thrust belts described by Butler and Paton (2010, p.9).

A number of variables may result in different layer-parallel compaction calculations between natural seismic and outcrop examples (noted above) which typically show an increase in compaction towards the sediment surface, and experimental sandbox models (e.g. Koyi et al., 2004) that display a reduction upwards through the model. Teixell and Koyi (2003) undertook sandbox experiments using a combination of glass microbeads and sand that display 18-32% layer-parallel compaction. However, layers composed of glass microbeads displayed less layer-parallel shortening, principally due to the packing properties of glass spherules that compact less than the sub-angular quartz sand (Teixell and Koyi, 2003). Thus, it appears that layer-parallel compaction in models is primarily accommodated through porosity reduction (Koyi et al., 2004).

We suggest that these conflicting patterns of layer parallel compaction, which increases towards the sediment surface in nature, and reduces towards the top of experiments may relate to; 1) More heterogeneous lithologies in nature compared to sand boxes; 2) Expulsion of pore fluids in nature (that don't exist in sand boxes); 3) The recognition in many sand box experiments that "the amount of layer parallel compaction observed in the models does not equate to the (greater) amount of layer parallel shortening in a natural case" (Koyi et al. (2004, p. 218). 4) Increasing vertical compaction down a natural sediment pile that does not effectively exist in a cm-scale sandbox. The effect of vertical compaction associated with overburden loading is typically to expel pore fluids, reduce porosity and thereby increase the strength of the sediment with depth.

In summary, line-length balancing in the case study reveals significant reductions in fold and thrust shortening up through slump systems that we attribute to increasing (by ~10%) heterogeneous lateral compaction towards the sediment surface (Fig. 12). The bulk amount of lateral compaction through the entire sequence is likely to be significantly greater, with some estimates from seismically imaged offshore fold and thrust belts placing this figure as high as 40% (Butler and Paton, 2010). We suggest that in the case study MTDs, the increasing component of layer-parallel compaction towards the sediment surface reflects increasing porosity reduction associated with lateral compaction in the upper parts of the sediment pile. These uppermost sections (typically within ~1 m of the sediment / water interface) have largely escaped vertical compaction linked to depositional overburden loading, and are therefore more susceptible to porosity reduction associated with later horizontal layer-parallel compaction.

The precise timing of layer-parallel compaction within the deformational sequence is open to debate. As fold and thrust systems maintain typical angular relationships and pristine geometries, any heterogeneous lateral compaction must have occurred at the very earliest stages of slumping prior to fold and thrust initiation (see also Butler and Paton, 2010). Upright folding that could be attributed to such lateral shortening is interpreted to predate thrusts, as such folds are carried and passively rotated on back-steepened thrusts (Alsop and Marco, 2011). Early upright folding is also preserved at the extreme open-toes of slumps in areas where thrusts failed to propagate (Alsop et al., 2016b). Similar patterns were observed in the sand box models of Koyi (1995) and Koyi et al. (2004), where layer parallel compaction developed early in the structural sequence, particularly at the leading edge of the deformation front "where less-compacted sediments are accreted".

6.6. Do linked thrust systems in MTDs undergo constant rates of slip?

Chapman and Williams (1984) note that a change in gradient of points on cumulative displacement-distance (CD-D) graphs relates to a change in rate of slip along the floor fault. While straight line graphs indicate a constant rate of slip along the floor fault, profiles with concave curves represent variable slip rates along the floor fault. All CD-D graphs measured across imbricate systems display broadly linear relationships (Fig. 8), suggesting a constant rate of slip along the floor fault during its displacement history. In detail however, plots display a distinct steeper step in the CD-D profile, consistent with an interpretation of an increased rate of slip along the floor thrust (Fig 8c, d). This step could reflect the position of potential out of sequence thrusting (e.g. thrust 4 from Fig 8c shown in Fig. 2h), and/or thrusts with marked displacement gradients toward their tips (e.g. thrust 3 from Fig. 8d shown in Fig. 9h). The steps observed in CD-D plots from the present study are typically greater than the more gently curving plots from thrusts cutting lithified sequences (Chapman and Williams, 1984). The stepped profile in CD-D plots from Peratzim likely marks a component of variable slip along the floor thrust, once again highlighting the greater variability in thrusts cutting unlithified sediments.

6.7. What influences patterns of displacement along individual thrusts in MTDs?

It has previously been suggested that lithology may play a role in how thrusts propagate and resulting patterns of displacement along them (e.g. Chapman and Williams, 1985, p.759). Muraoka and Kamata (1983) analysed displacement along normal faults cutting Quaternary lacustrine sediments, and observed that values of displacement typically increased where faults cut more competent beds, and then decreased where the same fault cut less competent strata on each side. Muraoka and Kamata (1983, p.492) also noted that displacement was more constant in the competent horizons and more variable in the incompetent layers. Similar patterns have recently been recorded from thrusts cutting lithified rocks (Ferrill et al., 2016). Muraoka and Kamata (1983, p.492) also suggest that depending on stress concentrations, competent beds "may play a role as either initiators or inhibitors of faulting" resulting in variable slopes on displacement-distance plots, while "incompetent layers act as passive strain absorbers" resulting in constant slopes on displacement-distance plots. Irregular displacement profiles may thus be created by restricting propagation of a single fault across 'barriers' that are "partially dependent on lithology (or competency)" (Ellis and Dunlap, 1988, p.184). In summary, non-linear slopes, or inflections in displacement-distance (D-D) graphs, can be considered to represent variations in fault development resulting from a number of factors including changes in lithology (Williams and Chapman, 1983) and/or pre-existing strain that weakened the rock (Noble and Dixon, 2011, p.74).

The competency of the ~10 cm thick 'orange' detrital marker unit within the thrusted sequence at Peratzim is demonstrated by a more parallel (Class 1B) style of folding, greater displacement of this unit along thrust ramps, and the interpretation that thrusts initiate in this horizon and diminish up and downwards into adjacent aragonite-rich units (Fig. 12). Steps in displacement-distance profiles also correspond to this same stratigraphic level which as a more competent layer affects the thrust propagation. In general, D-D profiles display steeper gradients toward the surface where less competent sediments are preserved.

Dramatic displacement gradients observed at Peratzim, where thrusts tip-out into overlying sediments, is similar to the "abrupt displacement gradients at the fault tips in the bounding mud rock beds" (Ferrill et al., 2016). Thus, as noted by Hedlund (1997, p.254), displacement-distance graphs can not necessarily be used to predict the location of fault tips (as originally suggested by Williams and Chapman, 1983; Chapman and Williams 1984). This is especially true where thrusts cut unlithified sediments as D-D analysis is much more variable, and displacement gradients towards fault tips are more pronounced and potentially non-linear making meaningful extrapolation difficult.

In summary, displacement-distance plots of thrusts cutting unlithified sediments reveal that displacement is more variable with more pronounced displacement gradients towards fault tips than observed in faults cutting lithified sequences. In addition, mechanical stratigraphy associated with more competent detrital-rich beds may influence the fault profiles on D-D graphs.

6.8. How do critical taper angles in MTDs compare to those in accretionary complexes?

The critical taper model is used to predict the evolution and geometry of large-scale fold and thrust belts and accretionary complexes (e.g. Davis et al., 1983). The shape of the wedge is generally considered to reflect the strength of the material and friction along the basal detachment, with weak wedges associated with low-friction basal decollements being marked by relatively long narrow tapers (e.g. see Koyi et al., 2004).

In the case study, we provide bulk estimates of the critical taper angles by measuring the thickness of the deformed slump horizons at various distances up to 500 m along the MTDs. This thickness and distance data were presented in Alsop et al. 2016b (their fig. 7a), with the variation in thickness providing the taper angle above the sub-horizontal decollement for each slump. The taper angles of slumps 4, 5, and 6 determined in this study are 0.38°, 0.28° and 0.19° respectively. These angles are exceptionally low, and an order of magnitude less than taper angles for large scale fold and thrust belts forming accretionary wedges, such as observed in Taiwan where angles of 4.7° were recently calculated (e.g. Yang et al., in press). Given that the taper angles of MTDs in the case study are two orders of magnitude less than large-scale accretionary complexes, we suggest that the low taper angles in slumps that form MTDs are a consequence of a) exceptionally weak saturated sediments that form the fold and thrust 'wedge', b) low-friction basal detachments that follow 'easy-slip' sub-horizontal bedding horizons, c) an overlying water column in Lake Lisan that comprised relatively dense hyper-saline brines, and would facilitate and encourage slumping at lower critical taper angles for a given water depth (see fig. 4 in Yang et al., in press). In the case study area, the ratio of MTD thickness to downslope extent is ~1:250, while the across strike extent is ~1:100 (see Alsop and Marco, 2011). These ratios are significantly larger than in typical accretionary complexes and would also be a consequence of the exceptionally low critical taper angles.

7. Conclusions

7.1. Thrusts cutting unlithified sediments display greater variations in the relative thickness of hangingwall and footwall cut-offs (or stretch) compared to thrusts cutting lithified rocks.
Values of stretch, which compares the relative cut-off thickness of equivalent hangingwall and footwall sequences, may be as low as 0.3 along thrusts cutting unlithified sediments. This ratio is significantly less than the minimum 0.5 values reported from thrusts cutting lithified rocks, and reflects the extreme variation in stratigraphic thickness that may affect soft-sediment deformation (Fig. 12).

7.2. Fault-propagation folds in unlithified sediments display tighter interlimb angles compared to models developed for lithified sequences.
Interlimb angles of <60° are associated with thinning of the forelimb, whereas interlimb angles of >90° occur with pronounced (>60%) forelimb thickening (Fig. 12). We suggest that the simple shear component of deformation in unlithified sediments modifies the forelimb thickness and interlimb angles to a greater extent than in lithified rocks.

7.3. Thrust ramps within slumps initiate in relatively competent horizons in the hangingwall of the underlying detachment.
Relatively competent units cut by thrust ramps may display the greatest displacement, which then progressively reduces both upwards and downwards along the ramp. This relationship suggests that ramps do not necessarily propagate upward from the underlying flat, but rather initiate in relatively competent horizons in the hangingwall of the detachment (Fig. 12).

Continued displacement along thrust ramps may however subsequently mask original displacement patterns, resulting in simple ‘steps’ in D-D graphs.

7.4. In slumps associated with MTDs, the average spacing of thrust ramps and the thickness of the thrust sequence displays an approximate 5:1 ratio across a range of scales.
Thicker hangingwall and footwall sequences are in general associated with larger thrust displacements, although displacement patterns on thrusts cutting unlithified sediments are more variable than those cutting lithified rocks.

7.5. Thrust systems within slumps and MTDs broadly balance, although heterogeneous lateral compaction may increase by ~10% towards the surface.
More than 40% shortening is observed within some fold and thrust systems at Peratzim. However, a 23% reduction in the amount of shortening taken up by folding and thrusting along individual thrusts suggests that heterogeneous lateral compaction may increase by ~10% toward the surface (Fig. 12). We suggest that sediment towards the top of the depositional pile that has undergone less compaction and overburden loading during deposition, will then be more prone to lateral compaction and horizontal shortening during subsequent slope failure associated with MTDs.

7.6. Linked thrust systems cutting unlithified sediments display distinct steps in cumulative displacement-distance (CD-D) plots representing increased rates of slip along the floor thrust. The stepped profile in CD-D graphs from thrusts cutting unlithified sediments likely marks a component of variable slip along the floor thrust, once again highlighting a greater inconsistency when compared to thrusts cutting lithified rocks.

7.7. Thrusts cutting more competent horizons in unlithified sediments are marked by ‘horizontal steps’ in displacement-distance (D-D) graphs.
Mechanical stratigraphy associated with more competent detrital-rich beds influences the fault profiles on D-D graphs (Fig. 12). D-D graphs also illustrate that thrusts cutting unlithified sediments display more variable displacement, and more pronounced displacement gradients toward fault tips, compared to thrusts cutting lithified sequences.

7.8. Critical taper angles in MTDs may be an order of magnitude less than those in accretionary complexes.
Exceptionally low critical taper angles in MTDs are considered a consequence of weak saturated sediments translating on low-friction basal detachments. This results in extreme ratios of MTD thickness compared to their downslope extent, with these ratios being significantly larger than in typical accretionary complexes.

Acknowledgements

GIA acknowledges funding from the Carnegie Trust to undertake fieldwork for this project. SM acknowledges the Israel Science Foundation (ISF grant No. 1436/14) and the Ministry of National Infrastructures, Energy and Water Resources (grant #214-17-027). RW was supported by the Israel Science Foundation (ISF grant No. 1245/11). We would like to thank

Hemin Koyi and Scott Wilkins for careful and constructive reviews, together with the editor Bill Dunne, for efficient handling of the manuscript.

Fig. 1 a) Tectonic plates in the Middle East. General tectonic map showing the location of the present Dead Sea Fault (DSF). The Dead Sea Fault is a left-lateral fault between the Arabian and African (Sinai) plates that transfers the opening motion in the Red Sea to the Taurus – Zagros collision zone with the Eurasian plate. Location of b) shown by the small box on the DSF. b) Map of the Dead Sea showing the position of the strands of the Dead Sea Fault (based on Sneh and Weinberger, 2014). The black arrows represent the direction of slumping in MTDs within the Lisan Formation, and form an overall semi-radial pattern around the western margin of Dead Sea Basin. The location of the study area shown in c) is boxed. c) Image of the light-coloured Lisan Formation at the Amiaz Plain, with the brownish Cretaceous margin to the west and the Sedom salt wall to the east. The box shows the location of the detailed case study area at Peratzim. Location grid relates to the Israel Coordinate System. d) Schematic 3-D diagram illustrating the position of the study area in the Amiaz Plain, located between the Dead Sea western border fault zone and the Sedom salt wall to the east. The thickness of the Lisan Formation has been exaggerated.

Fig. 2 Photographs of a) Slump 5, b) Slump 4, c) Slump 4 from Peratzim (N 31º0449.6 E 35º2104.2). Note that thrust numbering is for reference and does not imply order of ramp development. Stereonets of d) Slump 5 thrust planes (N=13), and folds (N=33), showing mean thrust plane (129/22W), mean fold hinge (2/317) and mean axial plane (139/13W) orientations (see Fig. 2a). e) Slump 4 thrust planes (N=5), and folds (N=12), showing mean thrust plane (005/16W), mean fold hinge 1/198, and mean axial plane (002/12W) orientations (see Fig. 2b). f) Slump 4 thrust planes (N=13), and folds (N=23), showing mean thrust plane (162/9W), mean fold hinge (9/172), and mean axial plane (177/12W) orientations (see Fig. 2c). Structural data on each stereonet is represented as follows: fold hinges (solid blue circles), mean fold hinge (open blue circle), poles to fold axial planes (open blue squares), poles to thrust planes (solid red squares) and mean axial plane (red great circle). Calculated slump transport directions based on fold data (blue arrows) and thrust data (red arrows) are subparallel to the trend of the outcrop section (black arrows). g, h) Photographs of Slumps 5 and 6 respectively, showing piggyback and out-of-sequence thrusting. In g), the displaced detrital-rich marker horizon is highlighted by orange squares (footwall) and circles (hangingwall).

Fig. 3 Schematic cartoon illustrating the main structural parameters and definitions of bed thicknesses measured around fault-propagation folds and thrusts.

Fig. 4 a) Graph comparing the stratigraphic thickness of thrust sequences with amount of displacement across the thrust (N=60). b) Graph showing that footwall thicknesses are always greater than the equivalent sequence in the hangingwall (N=57). c) Mean displacement versus mean thickness of hangingwall and footwall sequences from 16 different imbricate sequences throughout the study area. d) Data (N=8) from the Slump 5 thrust section (Fig. 2a) showing correlation of stretch with thickness of hangingwall sequence. e) Stretch versus displacement magnitude (Slump 5, Fig. 2a). f) Graph showing thickness of a stratigraphic sequence versus the average distance between thrust ramps. Data is based on 19 different imbricated sequences from the study area. Refer to Fig. 3 for definitions of thicknesses and parameters.

Fig. 5 a) Dip-isogon analysis of different layers forming a hangingwall anticline developed above Thrust 2 (T2) in Slump 5 (see Figure 2a for position). The detrital-rich horizon is marked in orange. Dip isogons join points of equal dip on adjacent folded surfaces, t_0 is layer thickness measured along the axial surface, while t_α is orthogonal layer thickness measured at various angles (α) to the axial surface. Representative 70° and 45° dip isogons are drawn on the upper and lower limbs of the fold respectively. b) t'α plot used to discriminate different classes of folds (see Ramsay, 1967, p.361 and Fossen, 2016, p.263. for details of technique). Colours relate to those in Fig. 5a, with upper fold limbs represented by coloured squares and lower limbs by circles. Detrital-rich units (in orange) more closely maintain layer thickness from the hinge to limbs of the fold, while aragonite-rich units display more extreme variations in layer thickness. c) Data from Slump 5 (Fig. 2a) showing that as % thickening of fold forelimbs occur (when compared to the backlimb thickness), there is a corresponding increase in the fold interlimb angle. Note that thrust numbering is for reference and does not imply order of ramp development.

Fig. 6 Fault-propagation-fold charts based on the models of Jamison (1987). a) Fault-propagation folds shown in Fig. 2c. b) Fault-propagation folds shown in Fig. 2b. c) Fault-propagation folds shown in Fig. 2a. In each case, the fault-propagation fold number is given in the circle (see Fig. 2 for photographs of corresponding structures), while the observed % of forelimb thinning (-ve) or thickening (+ve) is shown in blue or red respectively. Refer to Fig. 3 for definitions of thicknesses and parameters.

Fig. 7 a) Photograph, b) interpreted line drawing and c) line-length balanced cross section across a fold and thrust system (see Fig. 2a). Note that due to the length of the restored section (c), it is shown as three partially overlapping sections. Major thrust ramps cutting the competent 'orange' marker are numbered T1-T9, and the underlying floor thrust, are highlighted in red. Note that thrust numbering is for reference and does not imply order of ramp development. Cross section is within 5° of the calculated thrust transport direction (see Fig. 2d). A deficit in shortening is preserved in the upper green marker layer (see Table 1).

Fig. 8 Cumulative displacement-distance (CD-D) graphs (a-d), with numbers on graphs referring to thrust numbering on Figure 2. Note that thrust numbering is for reference and does not imply order of ramp development. a) CD-D graph from fold and thrust system shown in Fig. 2b. b) CD-D graph from fold and thrust system shown in Fig. 2c. c) CD-D graph from fold and thrust system shown in Fig. 2h). d) CD-D graph from fold and thrust system shown in Figs. 2a and 7.

Fig. 9 Photographs (a, c, e, g, i) and associated displacement-distance (D-D) graphs (b, d, f, h, j) across thrusts in Slump 5. In the photographs, displaced horizons are marked by matching coloured squares (footwall) and circles (hangingwall), with displacement decreasing to the fault tip (yellow circle). The associated D-D graphs show the hangingwall cut-off markers (coloured circles) defining a displacement profile drawn downward from the fault tip (yellow circle) at the origin. The 10 cm thick detrital-rich competent horizon is highlighted by an orange marker in each case (as also shown in Figs 5, 7). Refer to Figures 2a and 7 for details of thrust numbering.

Fig. 10 Photographs (a, b, d, f) and associated displacement-distance plots (c, e, g) across thrusts in Slump 4 (see Fig. 2b). In the photographs, displaced horizons are marked by matching coloured squares (footwall) and circles (hangingwall), with displacement decreasing to the fault tip (yellow circle). The associated D-D graphs show the hangingwall cut-off markers (coloured circles) defining a displacement profile drawn downwards from the fault tip (yellow circle) at the origin. Thicker detrital-rich competent horizons are highlighted by an orange and black marker in each case. Refer to Figures 2b for details of thrust numbering.

Fig. 11 Photographs (a, b, d, f) and associated displacement-distance plots (c, e, g) across thrusts in Slump 4. In the photographs, displaced horizons are marked by matching coloured squares (footwall) and circles (hangingwall), with displacement decreasing to the fault tip (yellow circle). The associated D-D graphs show the hangingwall cut-off markers (coloured circles) defining a displacement profile drawn downwards from the fault tip (yellow circle) at the origin. Thicker detrital-rich competent horizons are highlighted by an orange and dark blue marker in each case. Refer to Figures 2c for details of thrust numbering.

Fig. 12 Schematic cartoon summarising linked fold and thrust geometries generated in a downslope verging slump system. Schematic displacement-distance (D-D) graph highlights variations in offset across competent horizons (orange and blue circles shown on evolving thrust ramp). Note that lateral compaction is only illustrated on the right-hand side of the diagram.

Table 1. Balanced line-length restoration values of linked fold and thrust system in Slump 5 (see Fig. 7).

Marker horizon	Present length	Restored length	Shortening (thrusts only)	Shortening (folds only)	Shortening (thrusts and folds)	Missing shortening (as a % of blue 39.2 m restored length)	Missing shortening (as a % of blue 16.4 m shortening)
Top Green	22.8 m	35.6 m	9.3 m (26.2%)	3.3 m (9.3%)	12.6 m (35.4%)	3.8 m (9.7%)	3.8 m (23.2%)
Middle Orange	22.8 m	38.8 m	13.6 m (35.1%)	2.4 m (6.2%)	16 m (41.2%)	0.4 m (1%)	0.4 m (2.4%)
Lower Blue	22.8 m	39.2 m	15.9 m (40.6%)	0.5 m (1.3%)	16.4 m (41.8%)	0 m (0%)	0 m (0%)

References,

Agnon, A., Migowski, C., Marco, S., 2006. Intraclast breccia layers in laminated sequences: recorders of paleo-earthquakes, in Enzel, Y., Agnon, A., and Stein, M., eds., New Frontiers in Dead Sea Paleoenvironmental Research, Geological Society of America Special Publication, p. 195-214.

Alonso, J.L., Teixell, A.1992. Forelimb deformation in some natural examples of fault-propagation folds. In: McClay, K. (Editor), Thrust Tectonics. Chapman and Hall. London. 175-180.

Alsop, G.I., Holdsworth, R.E. 1993. The distribution, geometry and kinematic significance of Caledonian buckle folds in the western Moine Nappe, northwestern Scotland. Geological Magazine 130, 353-362.

Alsop, G.I., Holdsworth, R.E. 2007. Flow perturbation folding in shear zones. In: Ries, A.C., Butler, R.W.H. & Graham, R.D. (Eds) Deformation of the Continental Crust: The legacy of Mike Coward. Geological Society, London, Special Publications, 272, 77-103

Alsop, G.I., Marco, S 2011. Soft-sediment deformation within seismogenic slumps of the Dead Sea Basin. *Journal of Structural Geology* **33,** 433-457.

Alsop, G.I., Marco, S. 2012a. A large-scale radial pattern of seismogenic slumping towards the Dead Sea Basin. *Journal of the Geological Society* **169,** 99-110.

Alsop, G.I., Marco, S. 2012b. Tsunami and seiche-triggered deformation within offshore sediments. *Sedimentary Geology* 261, 90-107.

Alsop, G.I., Marco, S. 2013. Seismogenic slump folds formed by gravity-driven tectonics down a negligible subaqueous slope. *Tectonophysics* 605, 48-69.

Alsop, G.I., Marco, S. 2014. Fold and fabric relationships in temporally and spatially evolving slump systems: A multi-cell flow model. *Journal of Structural Geology*, 63, 27-49.

Alsop, G.I., Weinberger, R., Levi, T., Marco, S. 2015. Deformation within an exposed salt wall: Recumbent folding and extrusion of evaporites in the Dead Sea Basin. Journal of Structural Geology, 70, 95-118.

Alsop, G.I., Weinberger, R., Levi, T., Marco, S. 2016a. Cycles of passive versus active diapirism recorded along an exposed salt wall. Journal of Structural Geology 84, 47-67.

Alsop, G.I., Marco, S., Weinberger, R., Levi, T. 2016b. Sedimentary and structural controls on seismogenic slumping within Mass Transport Deposits from the Dead Sea Basin. Sedimentary Geology 344, 71-90.

Arkin, Y., Michaeli, L., 1986. The significance of shear strength in the deformation of laminated sediments in the Dead Sea area. Israel Journal of Earth Sciences 35, 61-72.

Armandita, C., Morley, C.K., Rowell, P. 2015. Origin, structural geometry, and the development of a giant slide: The South Makassar Strait mass transport complex. Geosphere, 11, 376-403. *doi:10.1130/GES01077.1*

Bartov, Y., Steinitz, G., Eyal, M., Eyal, Y., 1980. Sinistral movement along the Gulf of Aqaba - its age and relation to the opening of the Red Sea: Nature 285, 220-221.

Begin, Z.B., Ehrlich, A., Nathan, Y., 1974, Lake Lisan, the Pleistocene precursor of the Dead Sea: Geological Survey of Israel Bulletin, 63, p. 30.

Boyer, S.E., Elliot, D. 1982. Thrust systems. American Association of Petroleum Geologists Bulletin 66, 1196-1230.

Bull, S., Cartwright, J., Huuse, M. 2009. A review of kinematic indicators from mass-transport complexes using 3D seismic data. Marine and Petroleum Geology 26, 1132-1151.

Butler, R.W.H., 1987. Thrust sequences. Journal of the Geological Society, London, 144, 619-634.

Butler, R.W.H., Paton, D.A. 2010. Evaluating lateral compaction in deepwater fold and thrust belts: How much are we missing from "nature's sandbox"? GSA Today 20, 4-10.

Chapman, T.J., Williams, G.D. 1984. Displacement-distance methods in the analysis of fold-thrust structures and linked-fault systems. Journal of the Geological Society 141, 121-128.

Chapman, T., Williams, G., 1985. Strains developed in the hangingwall of thrusts due to their slip/propagation rate: a dislocation model: Reply. Journal of Structural Geology 7, 759-762.

Cooper, M. A., Garton, M.R., Hossack, J.R. 1982. Strain variation in the Hénaux Basse Normandie duplex, northern France. Tectonophysics 88, 321-323.

Corredor, F., Shaw, J.H., Bilotti, F., 2005. Structural styles in the deep-water fold and thrust belts of the Niger Delta. American Association of Petroleum Geologists Bulletin 89, 753-780.

Davis, D., Suppe, J., Dahlen, F.A. 1983. Mechanics of fold-and-thrust belts and accretionary wedges. Journal of Geophysical Research 88, (B2), 1153-1172.

Debacker, T.N., Dumon, M., Matthys, A. 2009. Interpreting fold and fault geometries from within the lateral to oblique parts of slumps: A case study from the Anglo-Brabant Deformation Belt (Belgium). Journal of Structural Geology 31, 1525-1539.

de Vera, J., Granado, P., McClay, K. 2010. Structural evolution of the Orange Basin gravity-driven system, offshore Namibia. Marine and Petroleum Geology 27, 223-237

Dotare, T., Yamada, Y., Adam, J., Hori, T., Sakaguchi, H. 2016. Initiation of a thrust fault revealed by analog experiements. Tectonophysics 684, 148-156.

Eisenstadt, G., DePaor, D.G. 1987. Alternative model of thrust fault propagation. Geology 15, 630-633.

El-Isa, Z.H., Mustafa, H. 1986. Earthquake deformations in the Lisan deposits and seismotectonic implications. Geophysical Journal of the Royal Astronomical Society 86, 413-424.

Ellis, M.A., Dunlap, W.J. 1988. Displacement variation along thrust faults: implications for the development of large faults. Journal of Structural Geology 10, 183-192.

Ferrill, D.A., Morris, A.P., Wigginton, S.S., Smart, K.J., McGinnis, R.N., Lehrmann, D. 2016. Deciphering thrust fault nucleation and propagation and the importance of footwall synclines. Journal of Structural Geology, 85, 1-11.

Fischer, M.W., Coward, M.P. 1982. Strains and folds within thrust sheets: an analysis of the Heilam sheet, northwest Scotland. Tectonophysics 88, 291-312.

Fossen, H. 2016. Structural Geology. 2nd Edition. Cambridge University Press, Cambridge, UK, p.510.

Frey Martinez, J., Cartwright, J., Hall, B. 2005. 3D seismic interpretation of slump complexes: examples from the continental margin of Israel. Basin Research 17, 83-108.

Garcia-Tortosa, F.J., Alfaro, P., Gibert, L., Scott, G. 2011. Seismically induced slump on an extremely gentle slope (<1°) of the Pleistocene Tecopa paleolake (California). Geology 39, 1055-1058.

Garfunkel, Z., 1981. Internal structure of the Dead Sea leaky transform (rift) in relation to plate kinematics: Tectonophysics 80, p. 81-108.

Garfunkel, Z., Ben-Avraham, Z. 1996. The structure of the Dead Sea basin. Tectonophysics 26, 155-176.

Gibert, L., Sanz de Galdeano, C., Alfaro, P., Scott, G., Lopez Garrido, A.C. 2005. Seismic-induced slump in Early Pleistocene deltaic deposits of the Baza Basin (SE Spain). Sedimentary Geology 179, 279-294.

Haase-Schramm, A., Goldstein, S.L., Stein, M. 2004. U-Th dating of Lake Lisan aragonite (late Pleistocene Dead Sea) and implications for glacial East Mediterranean climate change. Geochimica et Cosmochimica Acta 68, 985-1005.

Hedlund, C.A. 1997. Fault-propagation, ductile strain, and displacement-distance relationships. Journal of Structural Geology 19, 249-256.

Jackson, C. A-L. 2011. Three-dimensional seismic analysis of megaclast deformation within a mass transport deposit: implications for debris flow kinematics. Geology 39, 203-206.

Jacoby, Y., Weinberger, R., Levi, T., Marco, S. 2015. Clastic dikes in the Dead Sea basin as indicators of local site amplification. Natural Hazards 75, 1649-1676.

Jamison, W.R. 1987. Geometric analysis of fold development in overthrust terranes. Journal of Structural Geology 9, 207-219.

Jolly, B.A., Lonergan, L., Whittaker, A.C., 2016. Growth history of fault-related folds and interaction with seabed channels in the toe-thrust region of the deep-water Niger delta. Marine and Petroleum Geology 70, 58-76.

Kim, Y.S., Sanderson, D.J. 2005. The relationship between displacement and length of faults. Earth Science Reviews 68, 317-334.

Korneva, I., Tondi, E., Jablonska, D., Di Celma, C., Alsop, I., Agosta, F. 2016. Distinguishing tectonically- and gravity-driven synsedimentary deformation structures along the Apulian platform margin (Gargano Promontory, southern Italy). Marine and Petroleum Geology 73, 479-491.

Koyi, H. 1995. Mode of internal deformation in sand wedges. Journal of Structural Geology 17, 293-300.

Koyi, H.A., Sans, M., Teixell, A., Cotton, J., Zeyen, H. 2004. The significance of penetrative strain in the restoration of shortened layers – insights from sand models and the Spanish Pyrenees. In: McClay, K.R. (Editor) Thrust Tectonics and hydrocarbon systems. American Association of Petroleum Geology Memoir 82, 207-222.

Levi, T., Weinberger, R., Aîfa, T., Eyal, Y., Marco, S., 2006. Injection mechanism of clay-rich sediments into dikes during earthquakes: Geochemistry, Geophysics, and Geosystems, v. 7, no. 12, p. Q12009

Levi, T., Weinberger, R., Eyal, Y., Lyakhovsky, V., Hefez, E. 2008. Velocities and driving pressures of clay-rich sediments injected into clastic dykes during earthquakes. Geophysical Journal International 175, 1095-1107.

Liu, S., Dixon, J.M. 1995. Localization of duplex thrust-ramps by buckling: analog and numerical modelling. Journal of Structural Geology 17, 875-886.

Maltman, A. 1984. On the term soft-sediment deformation. Journal of Structural Geology 6, 589-592.

Maltman, A. 1994. Prelithification Deformation. In: Hancock, P.L. (Editor) Continental deformation. Pages 143-158. Pergamon Press.

Marco, S., Agnon, A. 1995. Prehistoric earthquake deformations near Masada, Dead Sea graben. *Geology*, 23, 695-698.

Marco, S., Kagan, E.J. 2014. Deformed sediments in the Dead Sea drill core: a long term palaeoseismic record. EGU General Assembly Conference Abstracts, vol. 16, 4375. Vienna.

Marco, S., Stein, M., Agnon, A., and Ron, H., 1996. Long term earthquake clustering: a 50,000 year paleoseismic record in the Dead Sea Graben: J. Geophys. Res., 101, 6179-6192.

Marco, S., Weinberger, R., Agnon, A., 2002, Radial clastic dykes formed by a salt diapir in the Dead Sea Rift, Israel: Terra Nova 14, 288-294.

McClay, K., 2011. Introduction to thrust fault-related folding. In McClay, K., Shaw, J.H., Suppe, J. (Eds.), Thrust-Fault-related Folding, 94, American Association of Petroleum Geologists Memoir, pp. 1-19.

McNaught, M.A., Mitra, G. 1996. The use of finite strain data in constructing a retrodeformable cross-section of the Meade thrust sheet, southeastern Idaho, U.S.A. Journal of Structural Geology 18, 573-583.

Morley, C.K. 1986. A classification of thrust fronts. American Association of Petroleum Geologists Bulletin 70, 12-25.

Morley, C.K., King, R., Hillis, R., Tingay, M., Backe, G. 2011. Deepwater fold and thrust belt classification, tectonics, structure and hydrocarbon prospectivity: A review. Earth Science Reviews, 104, 41-91.

Muraoka, H., Kamata, H., 1983. Displacement distribution along minor fault traces. Journal of Structural Geology 5, 483-495.

Noble, T.E., Dixon, J.M., 2011. Structural evolution of fold-thrust structures in analog models deformed in a large geotechnical centrifuge. Journal of Structural Geology 33, 62-77.

Ortner, H., Kilian, S. 2016. Sediment creep on slopes in pelagic limestones: Upper Jurassic of Northern Calcareous Alps, Austria. Sedimentary Geology. 344, 350-363.

Peacock, D.C.P., Sanderson, D.J. 1996. Effects of propagation rate on displacement variations along faults. Journal of Structural Geology 18, 311-320.

Peel, F.J., 2014. The engines of gravity-driven movement on passive margins: Quantifying the relative contribution of spreading vs. gravity sliding mechanisms. Tectonophysics 633, 126-142.

Porat, N., Levi, T., Weinberger, R. 2007. Possible resetting of quartz OSL signals during earthquakes – evidence from late Pleistocene injection dikes, Dead Sea basin, Israel. Quaternary Geochronology2, 272-277.

Prasad, S., Negendank, J.F.W., Stein, M. 2009. Varve counting reveals high resolution radiocarbon reservoir age variations in palaeolake Lisan. Journal of Quaternary Science 24, 690-696.

Ramsay, J.G. 1967. Folding and fracturing of rocks. McGraw-Hill. New York. pp.568.

Ramsay, J.G., Huber, M.I. 1987. The techniques of modern structural geology. Volume 2. Academic Press, London. 309-700pp.

Reis, A.T., Araújo, E., Silva, C.G., Cruz, A.M., Gorini, C., Droz, L., Migeon, S., Perovano, R., King, I., Bache, F. 2016. Effects of a regional décollement level for gravity tectonics on late Neogene to recent large-scale slope instabilities in the Foz do Amazonas Basin, Brazil. Marine and Petroleum Geology 75, 29-52.

Rich, J.L. 1934. Mechanics of low-angle overthrust faulting as illustrated by Cumberland thrust block, Virginia, Kentucky and Tennessee. American Association of Petroleum Geologists Bulletin 18, 1584-1596.

Scarselli, N., McClay, K., Elders, C. 2016. Seismic geomorphology of Cretaceous megaslides offshore Namibia (Orange Basin): Insights into segmentation and degradation of gravity-driven linked systems. Marine and Petroleum Geology 75, 151-180.

Sharman, G.R., Graham, S.A., Masalimova, L.U., Shumaker, L.E., King, P.R. 2015. Spatial patterns of deformation and palaeoslope estimation within the marginal and central portions of a basin-floor mass-transport deposit, Taranaki Basin, New Zealand. Geosphere, 11, 266-306.

Sneh, A., Weinberger, R. 2014. Major structures of Israel and Environs, Scale 1:50,000. Israel Geological Survey, Jerusalem.

Sobiesiak, M., Kneller, B.C., Alsop, G.I., Milana, J.P. 2016. Internal deformation and kinematic indicators within a tripartite Mass Transport Deposit, NW Argentina. In press. Sedimentary Geology 344, 364-381.

Strachan, L.J., Alsop, G.I. 2006. Slump folds as estimators of palaeoslope: a case study from the Fisherstreet Slump of County Clare, Ireland. Basin Research 18, 451-470.

Suppe, J., Medwedeff, D.A. 1990. Geometry and kinematics of fault-propagation folding. Eclogae geol. Helv. 83/3 409-454.

Teixell, A., Koyi, H.A. 2003. Experimental and field study of the effects of lithological contrasts on thrust-related deformation. Tectonics 22, 1054. Doi: 10.1029/2002TC001407

Uzkeda, H., Poblet, J., Bulnes, M. 2010. A geometric and kinematic model for double-edge propagating thrusts involving hangingwall and footwall folding. An example from the Jaca-Pamplona Basin (Southern Pyrenees). Geological Journal 45, 506-520.

Van der Merwe, W.C., Hodgson, D.M., Flint, S.S. 2011. Origin and terminal architecture of a submarine slide: a case study from the Permian Vischkuil Formation, Karoo Basin, South Africa. Sedimentology 58, 2012-2038.

Weinberger, R., Levi, T., Alsop. G.I., Eyal, Y. 2016. Coseismic horizontal slip revealed by sheared clastic dikes in the Dead Sea basin. Geological Society of America Bulletin 128, 1193-1206.

Williams, G., Chapman, T. 1983. Strains developed in the hangingwall of thrusts due to their slip/propagation rate: a dislocation model. Journal of Structural Geology 5, 563-571.

Woodcock, N. H 1976a. Ludlow Series slumps and turbidites and the form of the Montgomery Trough, Powys, Wales. Proceedings of the Geologists Association 87, 169-182.

Woodcock, N. H 1976b. Structural style in slump sheets: Ludlow Series, Powys, Wales. Journal of the Geological Society, London 132, 399-415.

Woodcock, N.H. 1979. The use of slump structures as palaeoslope orientation estimators. *Sedimentology*, 26, 83-99.

Yang, C.M., Dong, J.J., Hsieh, Y.L., Liu, H.H., Cheng, L.L. (in press). Non-linear critical taper model and determination of accretionary wedge strength. Tectonophysics. Doi: 10.1016/j.tecto.2016.04.026

Zalan, P.V., 2005. End members of gravitational fold and thrust belts (GFTBs) in the deep waters of Brazil. In: Shaw, J.H., Connors, C., and Suppe, J., (Editors) An AAPG Seismic Atlas: AAPG studies in Geology 53, 147-156.

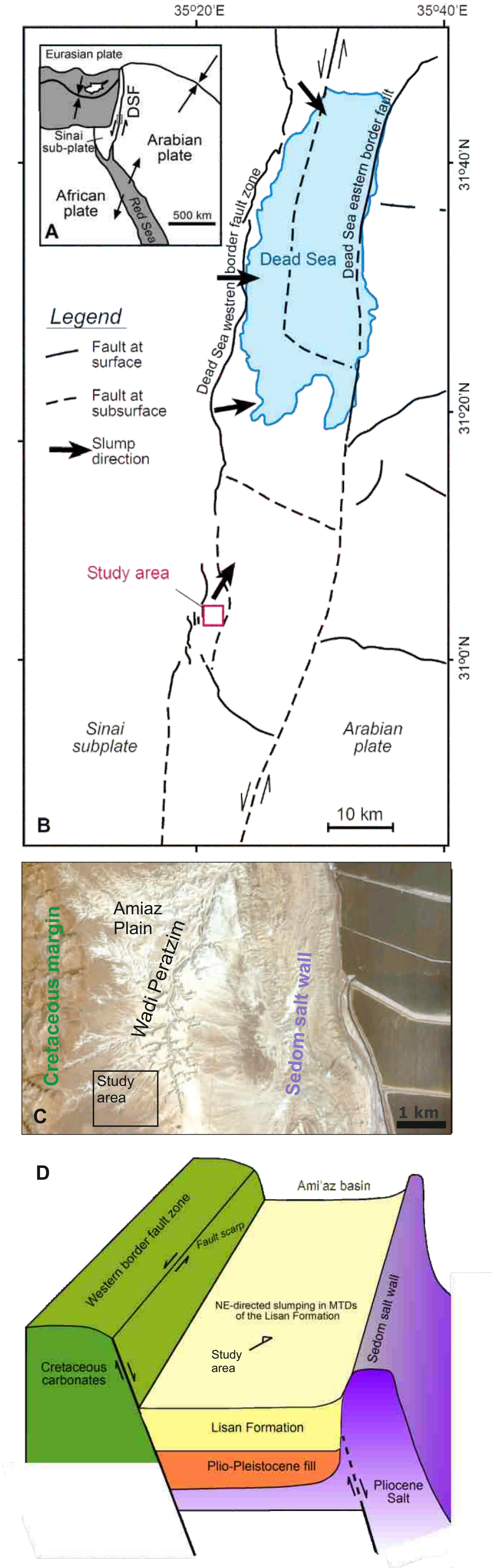

35°20'E
35°40'E
31°40'N
31°20'N
31°0'N
Eurasian plate
DSF
Sinai sub-plate
Arabian plate
African plate
Red Sea
500 km
A
Dead Sea
Dead Sea westren border fault zone
Dead Sea eastern border fault
Legend
Fault at surface
Fault at subsurface
Slump direction
Study area
Sinai subplate
Arabian plate
10 km
B
Amiaz Plain
Wadi Peratzim
Cretaceous margin
Sedom salt wall
Study area
1 km
C
D
Ami'az basin
Western border fault zone
Fault scarp
NE-directed slumping in MTDs of the Lisan Formation
Study area
Sedom salt wall
Cretaceous carbonates
Lisan Formation
Plio-Pleistocene fill
Pliocene Salt

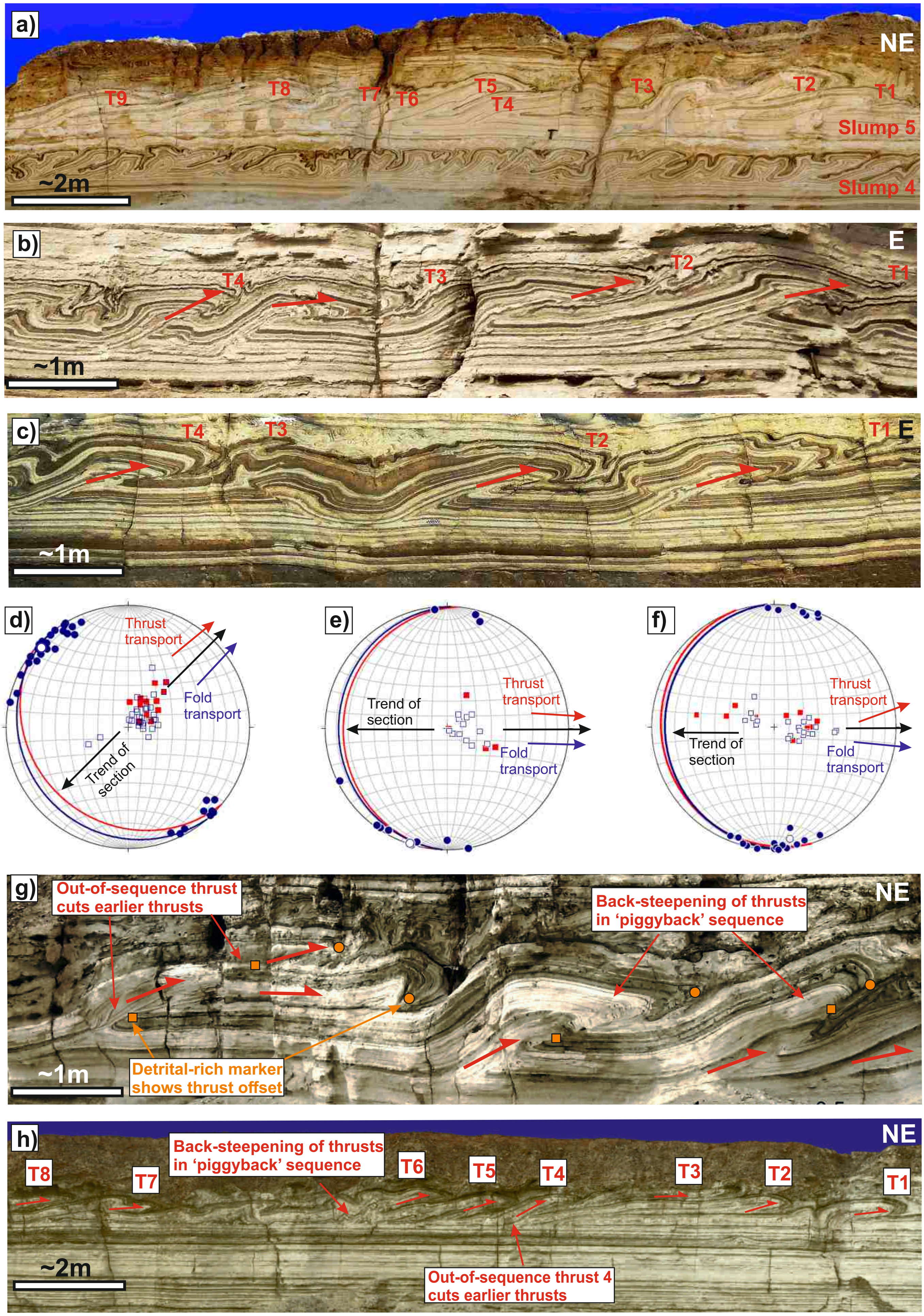

a)
NE
T9
T8
T7
T6
T5
T4
T3
T2
T1
Slump 5
Slump 4
~2m
b)
E
T4
T3
T2
T1
~1m
c)
T4
T3
T2
T1
E
~1m
d)
Thrust transport
Fold transport
Trend of section
e)
Trend of section
Thrust transport
Fold transport
f)
Thrust transport
Trend of section
Fold transport
g)
Out-of-sequence thrust cuts earlier thrusts
Back-steepening of thrusts in 'piggyback' sequence
NE
Detrital-rich marker shows thrust offset
~1m
h)
NE
T8
T7
Back-steepening of thrusts in 'piggyback' sequence
T6
T5
T4
T3
T2
T1
Out-of-sequence thrust 4 cuts earlier thrusts
~2m

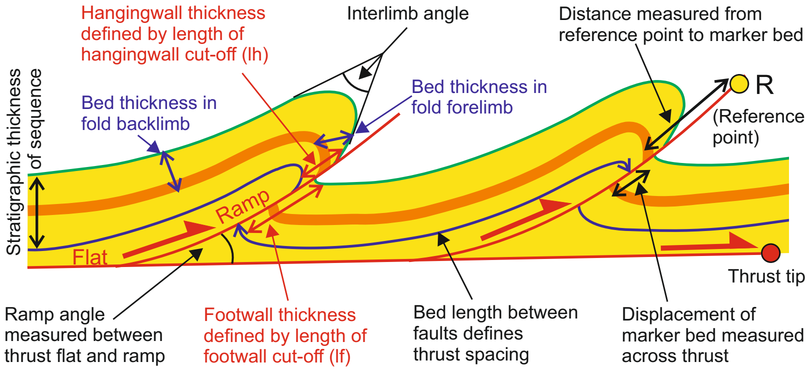

Hangingwall thickness
defined by length of
hangingwall cut-off (lh)
Interlimb angle
Distance measured from
reference point to marker bed
Stratigraphic thickness
of sequence
Bed thickness in
fold backlimb
Bed thickness in
fold forelimb
R
(Reference
point)
Ramp
Flat
Thrust tip
Ramp angle
measured between
thrust flat and ramp
Footwall thickness
defined by length of
footwall cut-off (lf)
Bed length between
faults defines
thrust spacing
Displacement of
marker bed measured
across thrust

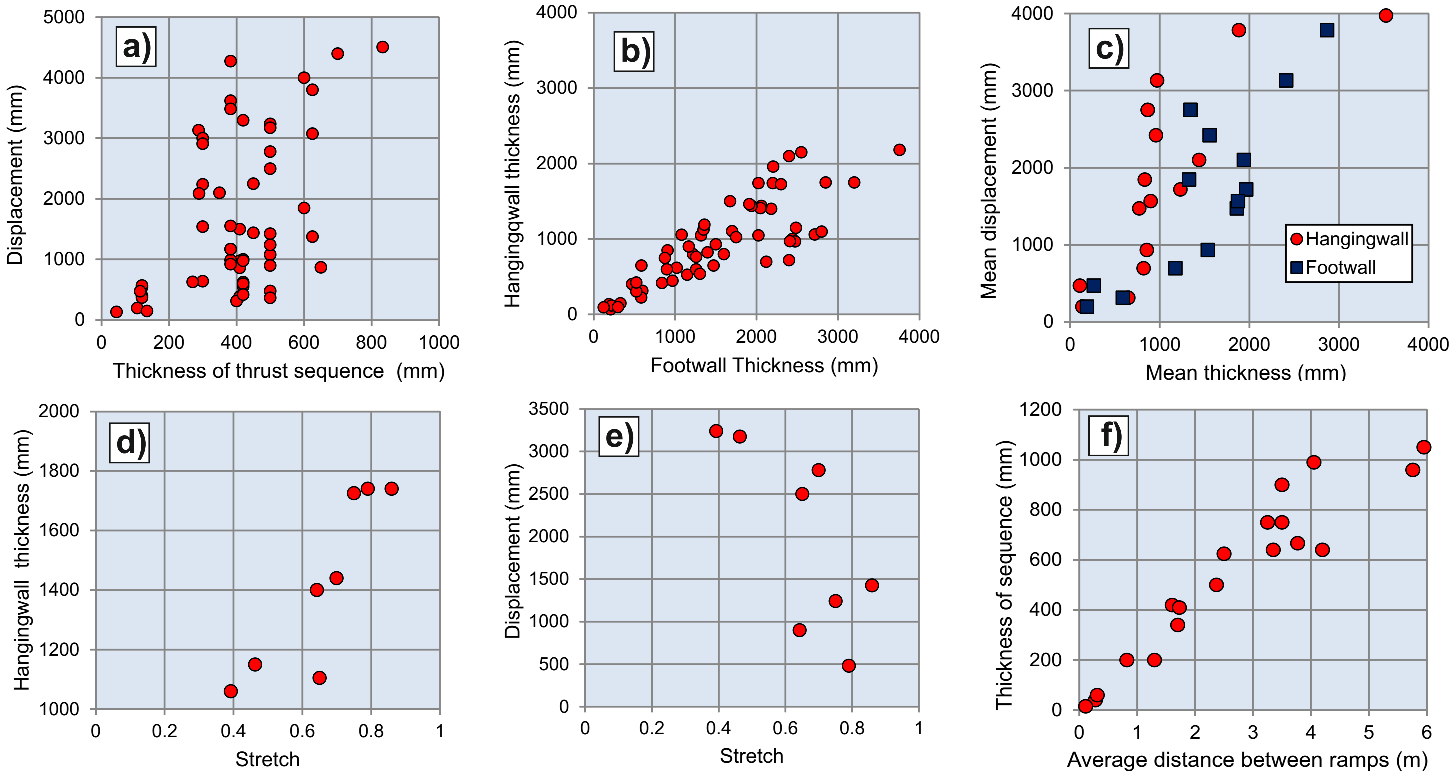

a)
Displacement (mm)
Thickness of thrust sequence (mm)
b)
Hangingwall thickness (mm)
Footwall Thickness (mm)
c)
Mean displacement (mm)
Mean thickness (mm)
Hangingwall
Footwall
d)
Hangingwall thickness (mm)
Stretch
e)
Displacement (mm)
Stretch
f)
Thickness of sequence (mm)
Average distance between ramps (m)

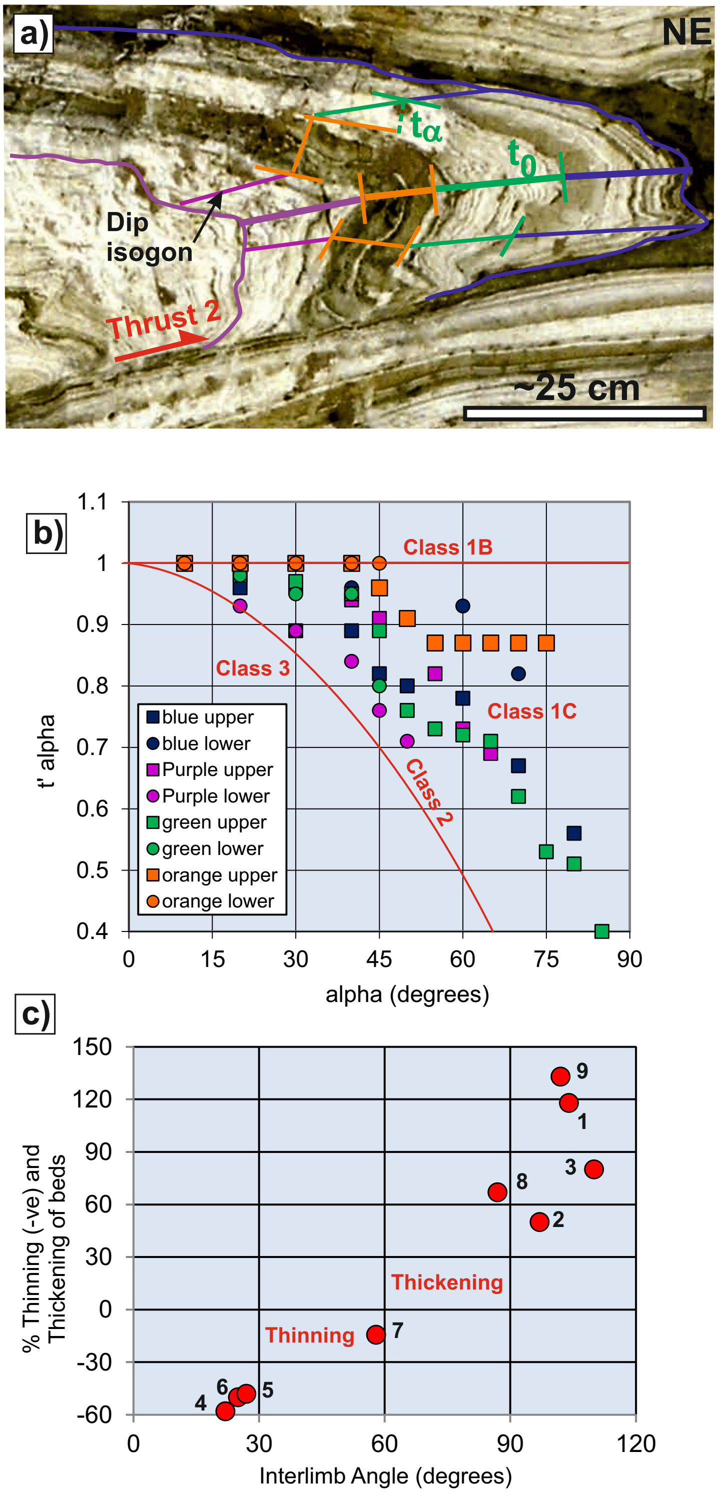
a)
NE
tα
t0
Dip
isogon
Thrust 2
~25 cm
b)
Class 1B
Class 3
Class 1C
Class 2
blue upper
blue lower
Purple upper
Purple lower
green upper
green lower
orange upper
orange lower
t' alpha
alpha (degrees)
c)
Thickening
Thinning
% Thinning (-ve) and Thickening of beds
Interlimb Angle (degrees)

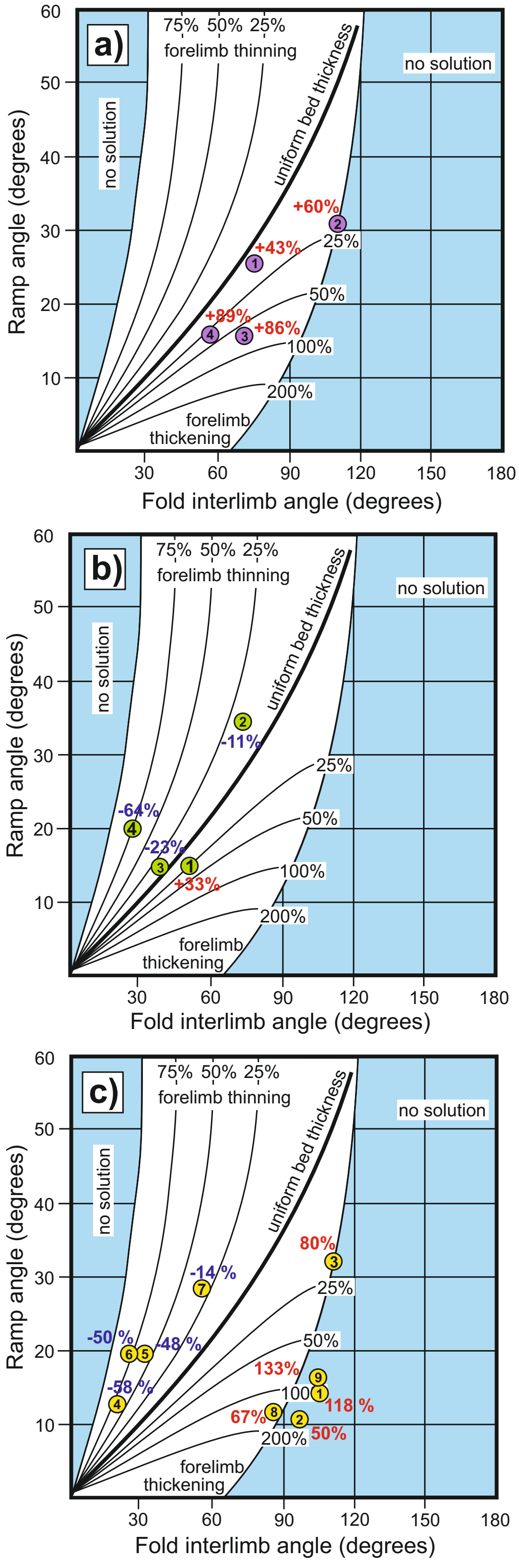

a)
b)
c)
75% 50% 25%
forelimb thinning
uniform bed thickness
no solution
no solution
forelimb
thickening
25%
50%
100%
200%
+60%
+43%
+89%
+86%
-11%
-64%
-23%
+33%
80%
-14 %
-50 %
-48 %
-58 %
133%
118 %
67%
50%
Ramp angle (degrees)
Fold interlimb angle (degrees)
10
20
30
40
50
60
30
60
90
120
150
180

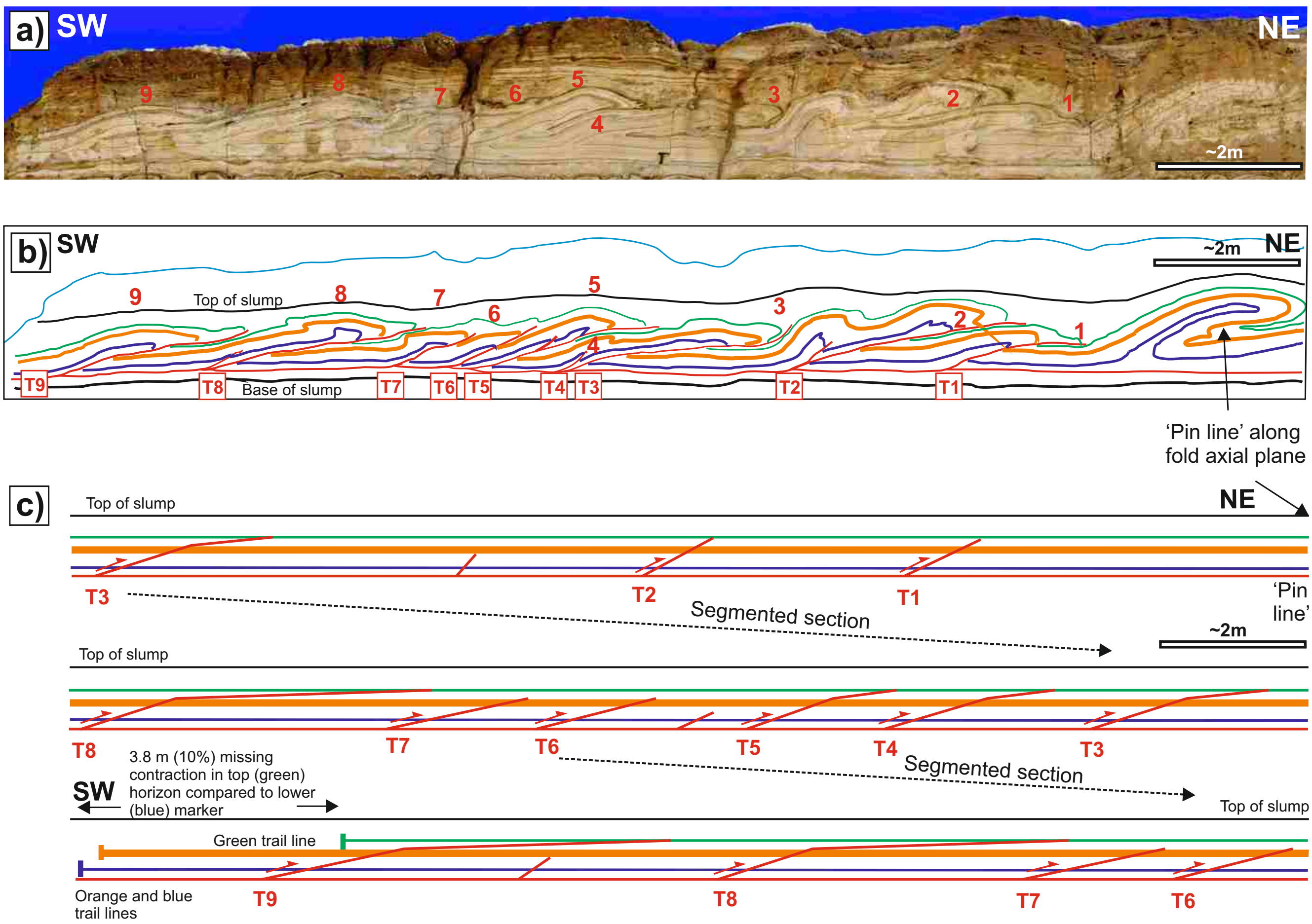
a) SW
NE
9
8
7
6
5
4
3
2
1
~2m
b) SW
NE
~2m
9
Top of slump
8
7
6
5
4
3
2
1
T9
T8
Base of slump
T7
T6
T5
T4
T3
T2
T1
'Pin line' along fold axial plane
c)
Top of slump
NE
T3
T2
T1
'Pin line'
Segmented section
~2m
Top of slump
T8
T7
T6
T5
T4
T3
3.8 m (10%) missing contraction in top (green) horizon compared to lower (blue) marker
Segmented section
SW
Top of slump
Green trail line
Orange and blue trail lines
T9
T8
T7
T6

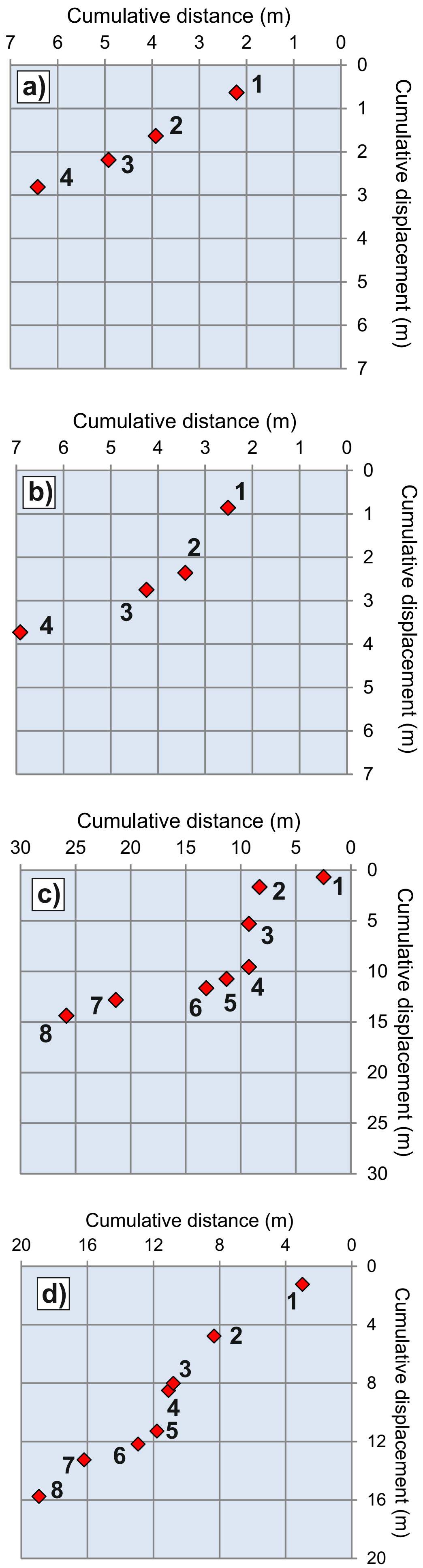

a)
Cumulative distance (m)
7 6 5 4 3 2 1 0
Cumulative displacement (m)
0 1 2 3 4 5 6 7
1
2
3
4
b)
Cumulative distance (m)
7 6 5 4 3 2 1 0
Cumulative displacement (m)
0 1 2 3 4 5 6 7
1
2
3
4
c)
Cumulative distance (m)
30 25 20 15 10 5 0
Cumulative displacement (m)
0 5 10 15 20 25 30
1
2
3
4
5
6
7
8
d)
Cumulative distance (m)
20 16 12 8 4 0
Cumulative displacement (m)
0 4 8 12 16 20
1
2
3
4
5
6
7
8

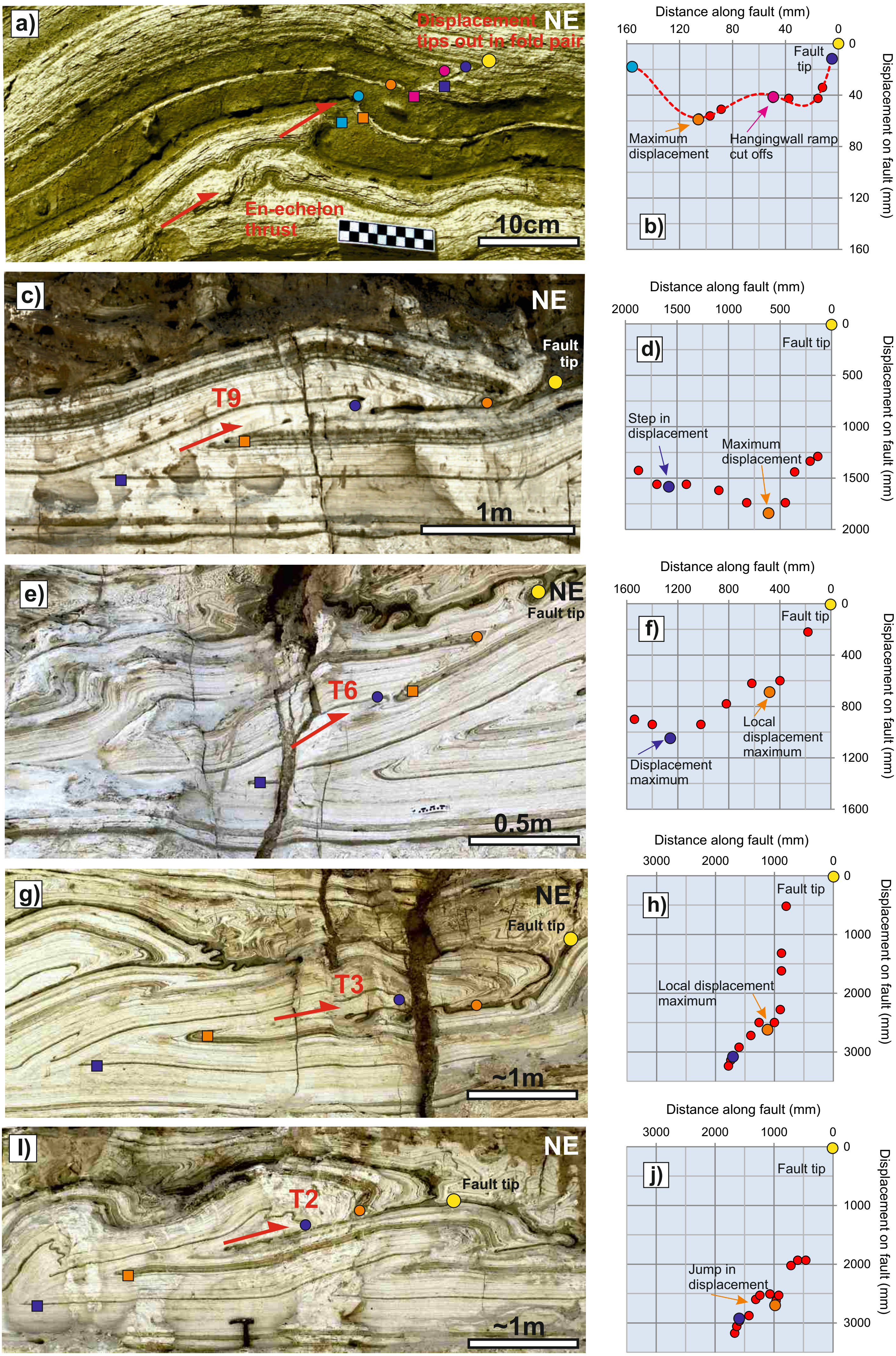

a)
NE
Displacement tips out in fold pair
En-echelon thrust
10cm
Distance along fault (mm)
160
120
80
40
0
Fault tip
Maximum displacement
Hangingwall ramp cut offs
b)
Displacement on fault (mm)
c)
NE
Fault tip
T9
1m
Distance along fault (mm)
2000
1500
1000
500
d)
Step in displacement
Maximum displacement
e)
NE
Fault tip
T6
0.5m
1600
1200
800
400
f)
Local displacement maximum
Displacement maximum
g)
T3
~1m
3000
2000
h)
Local displacement maximum
I)
T2
j)
Jump in displacement

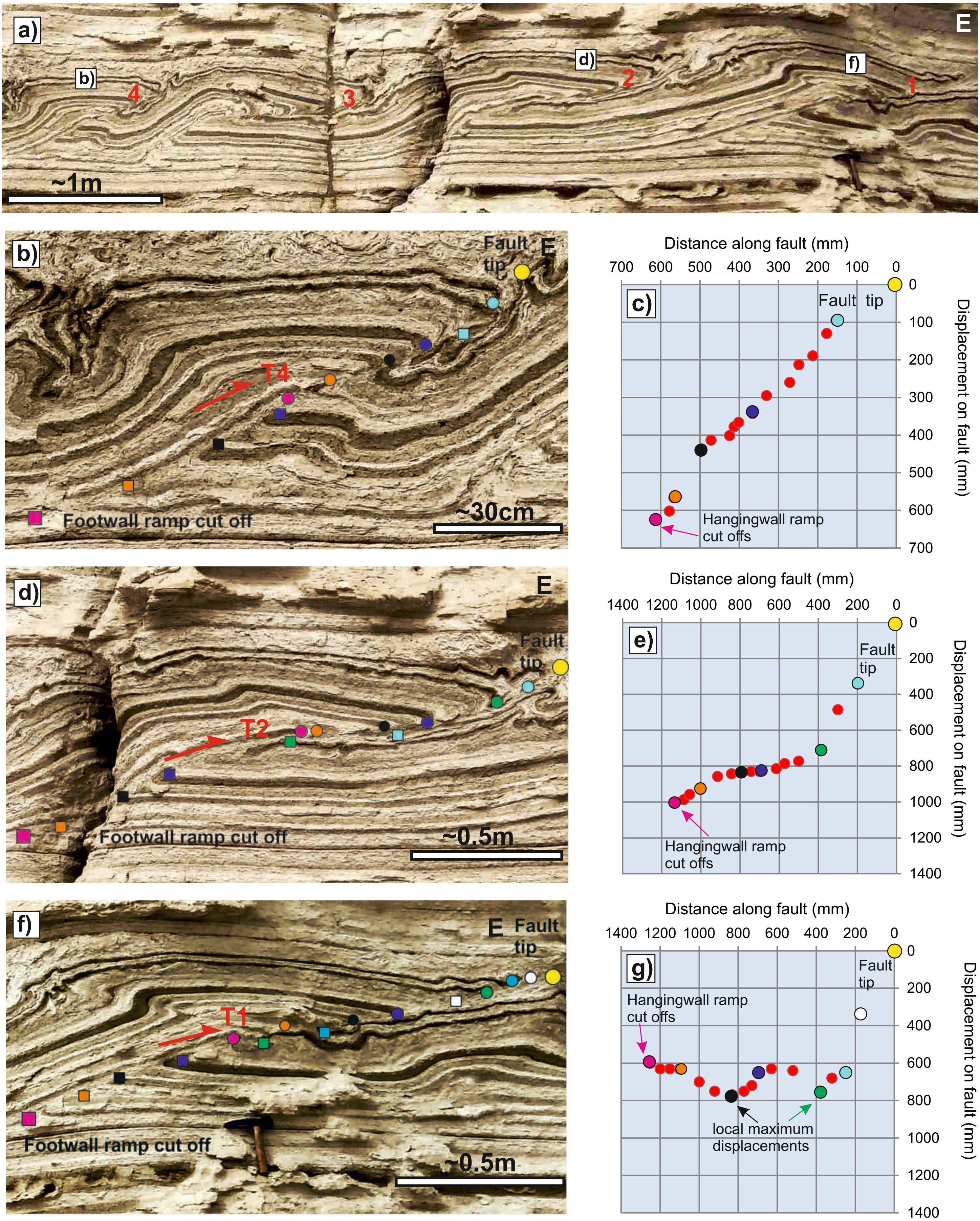

a)
E
b)
4
3
d)
2
f)
1
~1m
b)
Fault tip
E
T4
Footwall ramp cut off
~30cm
Distance along fault (mm)
700 600 500 400 300 200 100 0
c)
Fault tip
0
100
200
300
400
500
600
700
Displacement on fault (mm)
Hangingwall ramp cut offs
d)
E
Fault tip
T2
Footwall ramp cut off
~0.5m
Distance along fault (mm)
1400 1200 1000 800 600 400 200 0
e)
Fault tip
0
200
400
600
800
1000
1200
1400
Displacement on fault (mm)
Hangingwall ramp cut offs
f)
E
Fault tip
T1
Footwall ramp cut off
~0.5m
Distance along fault (mm)
1400 1200 1000 800 600 400 200 0
g)
Fault tip
Hangingwall ramp cut offs
local maximum displacements
0
200
400
600
800
1000
1200
1400
Displacement on fault (mm)

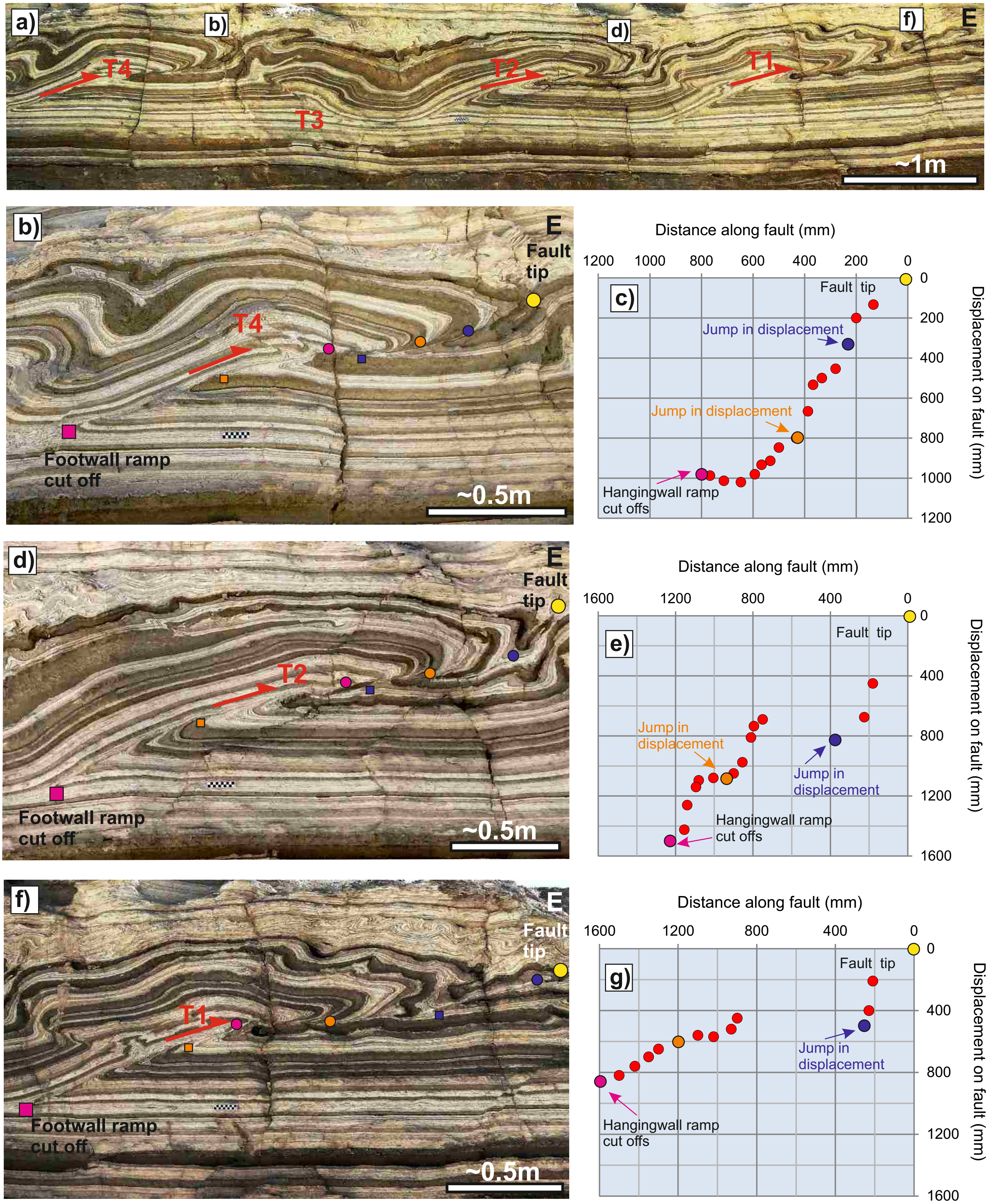

a)
b)
d)
f)
E
T4
T2
T1
T3
~1m
b)
E
Fault tip
T4
Footwall ramp cut off
~0.5m
Distance along fault (mm)
1200
1000
800
600
400
200
0
c)
Fault tip
Jump in displacement
Jump in displacement
Hangingwall ramp cut offs
Displacement on fault (mm)
0
200
400
600
800
1000
1200
d)
E
Fault tip
T2
Footwall ramp cut off
~0.5m
Distance along fault (mm)
1600
1200
800
400
0
e)
Fault tip
Jump in displacement
Jump in displacement
Hangingwall ramp cut offs
Displacement on fault (mm)
0
400
800
1200
1600
f)
E
Fault tip
T1
Footwall ramp cut off
~0.5m
Distance along fault (mm)
1600
1200
800
400
0
g)
Fault tip
Jump in displacement
Hangingwall ramp cut offs
Displacement on fault (mm)
0
400
800
1200
1600

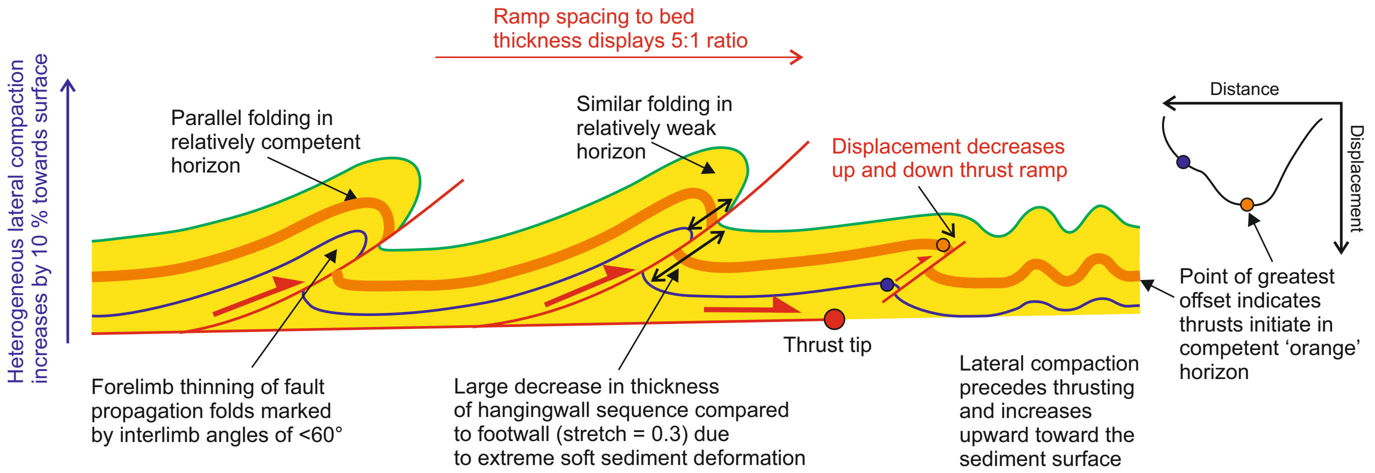
Heterogeneous lateral compaction increases by 10 % towards surface
Ramp spacing to bed thickness displays 5:1 ratio
Parallel folding in relatively competent horizon
Similar folding in relatively weak horizon
Displacement decreases up and down thrust ramp
Distance
Displacement
Point of greatest offset indicates thrusts initiate in competent 'orange' horizon
Thrust tip
Forelimb thinning of fault propagation folds marked by interlimb angles of <60°
Large decrease in thickness of hangingwall sequence compared to footwall (stretch = 0.3) due to extreme soft sediment deformation
Lateral compaction precedes thrusting and increases upward toward the sediment surface